

# The Physical Properties of Carbonaceous Asteroids

Daniel Britt

*University of Central Florida*

The rendezvous and sampling of asteroids 162173 Ryugu and 101955 Bennu have opened a new window on carbonaceous asteroid physical properties. Both objects have the structure of low-density rubble piles [1], with surfaces that are extremely rough, covered in starkly angular blocks and boulders, and depleted in fine particle sizes and dust [2]. The returned Ryugu material is similar to CI carbonaceous chondrites [3] and Bennu is likely either CI or CM-like materials. The surface of Ryugu exhibits very low thermal conductivity and high porosity [4]. What does this imply for the link between the physical properties of carbonaceous asteroids and hydrated carbonaceous meteorites?

The mineralogy these objects are dominated by phyllosilicates, primarily serpentines and saponite [3]. For Ryugu the serpentines are the magnesium-rich endmember similar to CI mineralogies. For Bennu the serpentine mineralogy is still unknown but may be the iron-rich endmember Cronstedtite. One major characteristic of serpentines is a strong negative excursion in the coefficient of linear thermal expansion in the range of 200°-250° K [5]. This effect is shown in Figure 1 for five CM carbonaceous chondrites. Since the carbonaceous materials are basically conglomerates that include some very dissimilar minerals, this negative thermal expansion excursion in serpentines may be key to understanding their surface properties as they evolve in the inner solar system. Cobbles and boulders exposed on the surfaces of carbonaceous asteroids will undergo extreme temperature excursions as they rotate into the Sun and then are exposed to deep space. All the minerals in the conglomerates will expand and contract according to their thermal expansion coefficients. For most minerals the expansion is a linear, positive function of temperature. However, for carbonaceous chondrites the serpentines and other phyllosilicates will expand, contract, and then expand again in a course of their heating and subsequent cooling. This will produce an extreme energetic effect on the mineral grain boundaries, essentially pushing them apart, contracting to open space, and then pushing apart again. The overall effect will be to weaken the conglomerate and induce increasing porosity into what appear to be coherent cobbles/boulders. This will leave the surface covered with boulders and cobbles that are extremely friable, porous, and weak. Because the effect is limited to the penetration depth of the rotational thermal pulse, it may be that only the surface materials are significantly weakened by this process. Cobbles buried at some modest depth and do not undergo temperature excursions may retain significantly more coherence and strength than the surface material.

One important observation is the lack of small particle size and dusty materials in the surface regolith. With the stresses induced by the thermal excursions, it would be expected that at least some of the boulder and cobble material would disaggregate to form a dusty regolith. However, the surface appears much like a “desert pavement” where active processes extract the fine materials from the surface and armor it with particle sizes too large to be moved by the active processes. Active ejection processes have been observed on Bennu with rocks as large as 10 cm being ejected. Because of the low gravity, fine particle sizes are likely to be entrained in the solar wind once ejected, resulting in a depletion of fines on the surface. Below the surface on both Ryugu and Bennu sampling activities revealed horizons more enriched in fine materials [1].

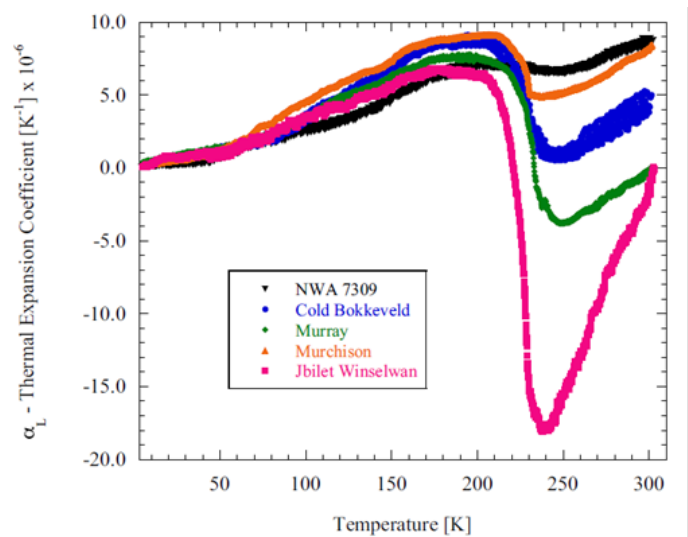


Figure 1. Thermal Expansion Coefficient for CM carbonaceous chondrites

## References

- [1] Sugita S. et al 2019. *Science* 364: 252 [2] Michikami T. et al. 2019. *Icarus* 331: 179. [3] Yokoyama T. et al. 2022. *Science* 10.1126/science.abn7850 [4] Gott M. et al. 2019 *Nature Astronomy* 3(11): 971. [5] Opeil C. et al. 2020. *MAPS* 10.1111/maps.13556. [6] Lauretta D. et al. 2019 *Science* 366:6470.

# New theoretical results on asteroid regolith specific heat, cohesion and heat transfer, and a revisit of comet 67P surface strength

J. Biele<sup>1</sup>, M. Grott<sup>2</sup>, S. Ulamec<sup>1</sup>, J. Knollenberg<sup>2</sup>, J.-B. Vincent<sup>2</sup>

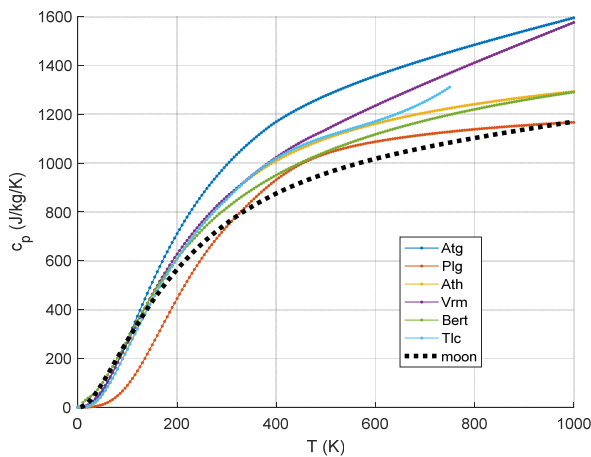
<sup>1</sup>German Aerospace Center, DLR-RB/MUSC Cologne, Germany

<sup>2</sup>German Aerospace Center, DLR-PF, Berlin, Germany

We report and discuss on some of our recent theoretical advances on asteroid regolith specific heat  $c_p$ , van der Waals-force between regolith particles, and heat transfer in the regolith. We also report on the strength of comet surface material, including a refined model of its size dependence and wide variability depending on the degree of “cementation” (sintering) and a re-appraisal of some particularly low and high strength values for comet 67P reported earlier in the literature. Thermal and mechanical properties are correlated.

## Specific heat

Surface temperature models could be impacted by the drastic decrease in  $c_p(T)$  values toward low temperatures; thermal models generally assume lunar basalt calorimetric properties, which are not well known outside the data range 90 K to 350 K. Indeed, ‘knowledge of specific heat variability as a function of temperature and bulk material composition remains largely



under-constrained for the need of planetary thermal modelers’[1].

In particular, the specific heat capacity of geological materials relevant to solar system body surfaces below room temperature is not particularly well constrained and the thermal modeling community only has a limited set of adequate ready-to-use  $c_p(T)$  trends for planetary surface temperature modeling. - We provide the means to calculate synthetic  $c_p(T)$  from a known bulk composition, for almost any solar system material from 10 K to 1000 K, and additionally a method to predict the specific heat curve beyond the temperature range measured, even if the composition is not (well) known. [2]

## Van-der-Waals force

[3] have calculated the pull-of force due to van der Waals interaction, and due to capillary bridges, between particles with self-affine fractal (random) roughness, which is realistic. They have shown that surface roughness, if big enough, results in an interaction (VdW) force which is independent of the size of the particles, in contrast to the linear size dependency expected for particles with smooth surfaces (simple JKR, DMT). For fractured rock particles a realistic surface roughness reduces the pull-of force between micrometer sized particles by a factor of  $\sim 100$ , and even more for larger particles, it is of the order of 0.1 – 1

nN. This means that the dependence of cohesive strength (or tensile strength, in  $N/m^2$ ) of the granular medium on particle size is due to the increase in the number of particle-particle contacts (per unit area) alone. A decrease in particle size only increases the number of contacts without changing the strength of the particle-particle adhesive bond. The small-particle glue idea, figure 1, of [4] is a good one! This results also affects the predicted (high) porosity of granular media in micro-gravity, since the granular Bond number is very different now.



The smallest particles form a “glue” or “cement” for the bigger particles

Force to break the bond between a small particle (diameter  $d \sim 6 \mu m$ ) and another particle =  $F_1$

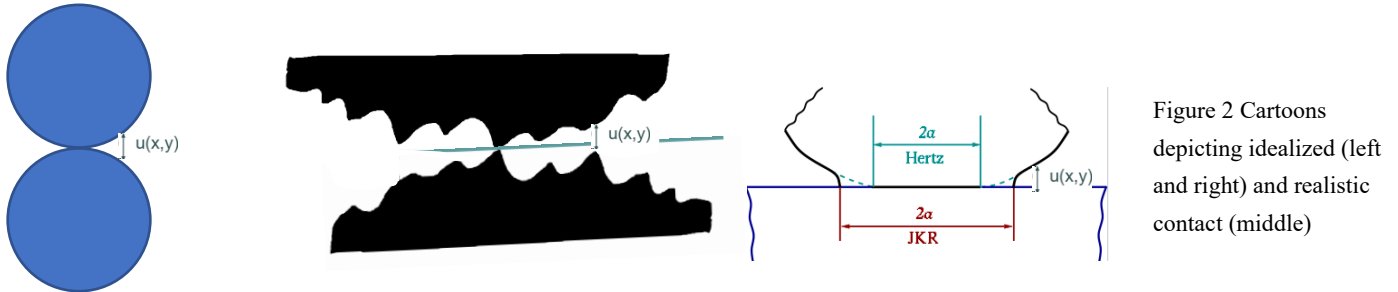
Yield stress in tension  $\sigma_y = \kappa F_1 / d^2$  where  $\kappa \sim 1$

If  $\sigma_y = 25 \text{ Pa}$  then  $F_1 \sim 1 \text{ nN}$

Figure 1. The big particles (fragments) in an asteroid could be kept together by a matrix of smaller particles. Effective yield stress of rubble pile asteroids of order (or less than)  $\sigma_y \approx 25 \text{ Pa}$ .

## Heat transfer

Thermal conductivity  $k$  of granular media and porous rocks seemed well explained by classical theories (Maxwell equations, Stefan-Boltzmann radiative transfer, contact mechanics like Hertz or JKR theory). All those classical thermal conductivity theories operate with models from the 19th century (Maxwell, Fourier, Stefan-Boltzmann law, Hertz) and completely neglect phonons and quantum mechanics! We are revising the underlying assumptions, and find that most are doubtful.



Rough irregular rock (silicate) particles do not form strong contacts when granular, not much phonon conduction across point contacts, JKR not applicable at all, heat transfer by near-field evanescent EM waves at least equally important, (NFRHT)  $\sim 1/R^{0.8}$ -dependence. Radiative conduction is not  $\propto T^3$  either, if grains are not well conducting (non-isothermality); different regime if void scale  $\leq$  thermal wavelength  $\lambda_T \approx 3000/T \mu\text{m K}$  (radiative transfer, dense media scattering and transmission, Planck not valid if particle size  $< \lambda_T$ ); Most assumptions on porosity dependence, in particular of  $k_{\text{rad}}$ , were wrong [5, 6]. Porous rock effective conductivity (meteorites) as function of porosity is not Maxwell „swiss cheese“, much lower values at medium porosities  $\rightarrow$  rather weakly cemented/sintered ex granular matter. Cracks, percolating and close pores, .. no theory is available! We are working both theoretically and experimentally to understand this better [7, 8].

## Revisit of Comet Surface Strength

For comet 67P, we have re-analyzed the data for the apparently exceptional 67P Abydos site, where originally a *lower* limit of several MPa for compressive strength was suggested. We use a correlation going back to Digby [9, 10] between strength, Young's module and thermal conductivity for weakly sintered porous media; our revised value for compressive strength is 28–690 kPa on the 5–30 cm scale, still representing the probably most competent material on the comet, potentially with a reduced porosity compared to the average 70–80%. The size effect law [11] for quasi-brittle failures bridging the small-size asymptotic strength (compressive or tensile) and the power law  $\sim 1/d^{1/2}$  of LEFM seems to apply for cometary and meteoritic material: the strength of very small lab samples cannot be simply extrapolated to larger sizes!

## **References**

- [1] Piqueux, S., et al., Journal of Geophysical Research: Planets, 2021. **126**(11): p. e2021JE007003. [2] Biele, J., et al., International Journal of Thermophysics, 2022. **43**(9): p. 144, DOI: 10.1007/s10765-022-03046-5. [3] Persson, B.N.J. and J. Biele, Tribology Letters, 2022. **70**(2): p. 34, DOI: 10.1007/s11249-022-01570-x. [4] Scheeres, D.J., C.M. Hartzell, and P. Sanchez, Icarus, 2010. **210**, DOI: 10.1016/j.icarus.2010.07.009. [5] Ryan, A.J., et al., Journal of Geophysical Research: Planets, 2020. **125**(2): p. e2019JE006100, DOI: 10.1029/2019je006100. [6] Ryan, A.J., et al., JGR Planets, 2022: p. e2022JE007191. [7] Persson, B.N.J. and J. Biele Applied Physics Letters, 2022, submitted. [8] Biele, J., et al., 44th COSPAR Scientific Assembly. Held 16-24 July, 2022. **44**: p. 186. [9] Digby, P., Journal of Applied Mechanics, 1981. **48**(4): p. 803-808. [10] Grott, M., et al., Nature Astronomy, 2019. **3**(11): p. 971-976. [11] Bažant, Z.P., Archive of Applied Mechanics, 1999. **69**(9-10): p. 703-725, DOI: 10.1007/s004190050252.

# Comparison of Thermal Inertia between Ryugu Sample and Carbonaceous Chondrites

Takuya Ishizaki<sup>1</sup>, Hosei Nagano<sup>2</sup>, Satoshi Tanaka<sup>1</sup>, Tatsuaki Okada<sup>1</sup>, Naoya Sakatani<sup>1</sup>, Tomoki Nakamura<sup>3</sup>, Ryohei Fujita<sup>2</sup>, Abdulkareem Alasli<sup>2</sup>, Tomoyo Morita<sup>3</sup>, Mizuha Kikui<sup>3</sup>, Kana Amano<sup>3</sup>, Eiichi Kagawa<sup>3</sup>, Hisayoshi Yurimoto<sup>4</sup>, Takaaki Noguchi<sup>5</sup>, Ryuji Okazaki<sup>6</sup>, Hikaru Yabuta<sup>7</sup>, Hiroshi Naraoka<sup>6</sup>, Kanako Sakamoto<sup>1</sup>, Shogo Tachibana<sup>8,1</sup>, Sei-ichiro Watanabe<sup>2</sup>, Yuichi Tsuda<sup>1</sup>

<sup>1</sup>Japan Aerospace Exploration Agency, 3-1-1 Yoshinodai, Sagamihara, Kanagawa 252-5210, Japan

<sup>2</sup>Nagoya University, Furo-cho, Chikusa-ku, Nagoya, Aichi, 464-8603, Japan

<sup>3</sup>Tohoku University, 2-1-1, Katahira, Aoba-ku, Sendai, Miyagi 980-8578, Japan

<sup>4</sup>Hokkaido University, 5, Kitahachijonishi, Kita-ku, Sapporo, Hokkaido 060-0810, Japan

<sup>5</sup>Kyoto University, Yoshidahonmachi, Sakyo-ku, Kyoto, Kyoto 060-0810, Japan

<sup>6</sup>Kyushu University, 6-10-1 Hakozaki, Higashi-ku, Fukuoka, Fukuoka 812-8581, Japan

<sup>7</sup>Hiroshima University, 1-3-2 Kagamiyama, Higashihiroshima, Hiroshima 739-8526, Japan

<sup>8</sup>The University of Tokyo, 7-3-1 Hongo, Bunkyo-ku, Tokyo 113-0033, Japan

**Introduction:** According to the general planetary formation scenario, the Solar System bodies evolved over a long period of time through repeated collision, fragmentation, and aggregation of planetesimals formed in the solar nebula. Thermal evolution, which induces various physicochemical reactions such as aqueous alteration, thermal metamorphism, and volcanism, is important for the evolution of planets. The temperature history inside the planetesimals followed in thermal evolution can vary greatly depending on when and how large they agglomerate and effective thermal conductivity. Therefore, it is essential for the theory of planetary system formation to know the thermal conductivity of asteroids and meteorites, especially those that are thought to have existed since the early stages of planetary system formation.

The Ryugu sample brought back in 2020 by Hayabusa2 was found to be a primitive Ivuna-type carbonaceous chondrite, which is close to the average composition of the Solar System [1]. Although it is expected that the physical properties of Ryugu, including thermal conductivity, will be analyzed in detail, most of the measurements of physical properties of meteorites have been performed on relatively easily available ordinary chondrites [2–4], because they require more samples than chemical and petrological evaluations. Therefore, there has been no method that can evaluate thermal conductivity of limited amount of samples such as Ryugu samples. In this study, we developed a lock-in thermography (LIT) periodic heating method that can measure the thermal diffusivity of small sample of several mm scale without contact [5]. Then we measured the anisotropic distribution of thermal diffusivity for five types of Ryugu samples. Additionally, Thermal inertia was evaluated using reported density and specific heat and compared with values reported for other carbonaceous chondrites.

**Samples and Methodology:** In this study, six samples of C0002-plate 3, C0002-plate 4, C0025, C0033, A0026 and A0064 were evaluated. C0002-plate 3 and C0002-plate 4 are flat plates cut out from C0002, and the others have granular shape. A spot on the sample is periodically heated using a laser and the temperature response is measured by LIT to obtain the phase lag distribution on the sample surface. The thermal diffusivity is analyzed from the gradient of the phase lag according to this equation;  $D = \pi f l (d\theta/dr)^2$ . Here,  $D$  is thermal diffusivity,  $f$  is heating frequency,  $\theta$  is phase lag and  $r$  is distance from heating point. Thermal inertia, which is expressed as the product of the square root of thermal diffusivity, density, and specific heat, was evaluated based on the reported density and specific heat. The heating frequency was selected according to the sample size to avoid the influence of reflected temperature waves at the sample edge, and then measurements were performed at 2, 1, 4, 4, 4, and 20 Hz for C0002-plate 3, C0002-plate 4, C0025, A0026, C0033, and A0064, respectively. C0002-plate 3, C0002-plate 4 and A0064 were measured under vacuum, and C0025, A0026, and C0033 were measured under atmospheric pressure because the vacuum environment was not available at that time yet. C0002-plate 4 was also measured under atmospheric pressure.

**Results and Discussion:** Figure 1 shows the phase lag distribution and the thermal diffusivity distribution of C0002-plate 3 as a representative of all samples. And the mean, maximum, minimum, and maximum to minimum ratio of the thermal diffusivity distribution for each sample are summarized in Table 1. C0002-plate 3 is known to have cracks in the evaluation region (in the direction of 105-195 deg), and it can be seen that the thermal diffusivity decreases significantly in the direction of the cracks. The other samples also show various thermal anisotropy. The results of C0002-plate 4 measured under both vacuum and atmospheric pressure show that the thermal diffusivity becomes larger, and the thermal anisotropy becomes smaller under atmospheric pressure. The thermal anisotropy seems to be caused by cracks inside the sample. Heterogeneity of mineral composition or microporosity may also affect. The returned Ryugu samples were found to have various mineral compositions and conglomerate-like structures [6].

Table 1. Measurement results of thermal diffusivity.

Sample	Average, mm <sup>2</sup> /s	Max/ Min, mm <sup>2</sup> /s	Max/Min ratio
C0002-3	0.28 ± 0.07	0.75/ 0.02	38.0
C0002-4 (Vacuum)	0.33 ± 0.08	1.05/ 0.07	15.0
C0002-4 (1 atm)	0.45 ± 0.12	0.60/ 0.31	1.94
C0025	0.56 ± 0.10	1.12/ 0.36	3.11
A0026	0.51 ± 0.02	0.60/ 0.34	1.76
C0033	0.58 ± 0.11	0.82/ 0.27	2.96

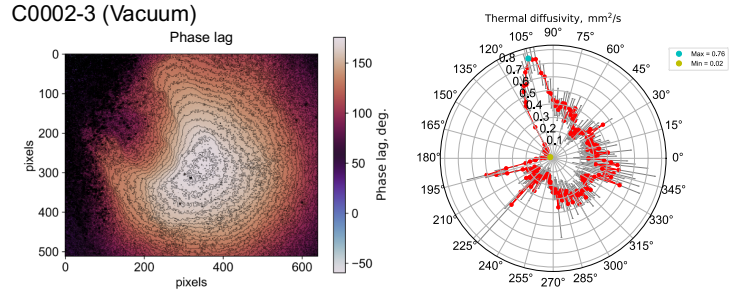


Figure 1. Phase lag and thermal diffusivity distribution of C0002-plate 3.

The obtained thermal diffusivity was then converted to thermal inertia using specific heat and bulk density, and a plot of the relationship with bulk density is shown in Figure 2. Error bars for thermal inertia indicate maximum and minimum values. The bulk densities of these samples are 1820, 1740, 1650, 2260, and 1870 kg/m<sup>3</sup> respectively, and the specific heat of 865 J/(kg · K) measured in the initial analysis was used as a representative value [6]. In addition, Figure 2 also shows plots of the thermal inertia of carbonaceous chondrites reported so far (Cold Bokkeveld (CM2), Jbilet Winselwan (CM2), Murchison (CM2), Murray (CM2), NWA 7309 (CM2), NWA 5515 (CK4), Allende (CV3), Kainsaz (CO3.2)) [4, 7]. The plots are shown in light blue for the measurements taken in vacuum and in purple for those taken at atmospheric pressure. The thermal inertia at atmospheric pressure becomes larger than that at vacuum pressure because the thermal diffusivity becomes larger due to the air-filled cracks.

The averaged values of the thermal inertia of 748-1475 J/(s<sup>1/2</sup>m<sup>2</sup>K) obtained in this measurement is significantly larger than that observed value of 300±100 J/(s<sup>1/2</sup>m<sup>2</sup>K) [8] by the thermal infrared imager (TIR) onboard Hayabusa2. On the other hand, some of the minimum values corresponded to the observed values. This suggests that the value of thermal inertia may differ depending on the measurement scale. In this measurement, the thermal diffusivity was evaluated in the region of several hundreds of micrometers long as thermal diffusion length, but the TIR observations were made at depths down to several centimeters because the thermal inertia was analyzed using the diurnal variation of the surface temperature due to the 7.6-hour rotation period of asteroid Ryugu. Therefore, it is possible that large-scale cracks caused by meteor impacts and thermal stresses on a scale larger than several hundreds of micrometers are widely developed in the rocks and boulders of Ryugu

The Ryugu sample seems to be the lowest-density category when compared to carbonaceous meteorites, and the thermal inertia values appear to follow a correlation trend with the bulk density of carbonaceous chondrites. However, if the bulk density of the Ryugu sample were 2236 kg/m<sup>3</sup>, which is the average of the five CM2 densities, the average thermal inertia of the Ryugu sample would be 1132 J/(s<sup>1/2</sup>m<sup>2</sup>K), which is almost identical to the average CM2 value of 1191 J/(s<sup>1/2</sup>m<sup>2</sup>K). This means that the only substantial difference between Ryugu and CM2 is the bulk density, and the product of thermal conductivity and specific heat are almost the same. Since the thermal conductivity generally decreases when the bulk density decreases due to porosity, it is possible that the thermal conductivity of Ryugu's matrix is larger than that of CM2. Further validation will be conducted by evaluating additional carbonaceous chondrites including CI chondrites, which are closest to Ryugu.

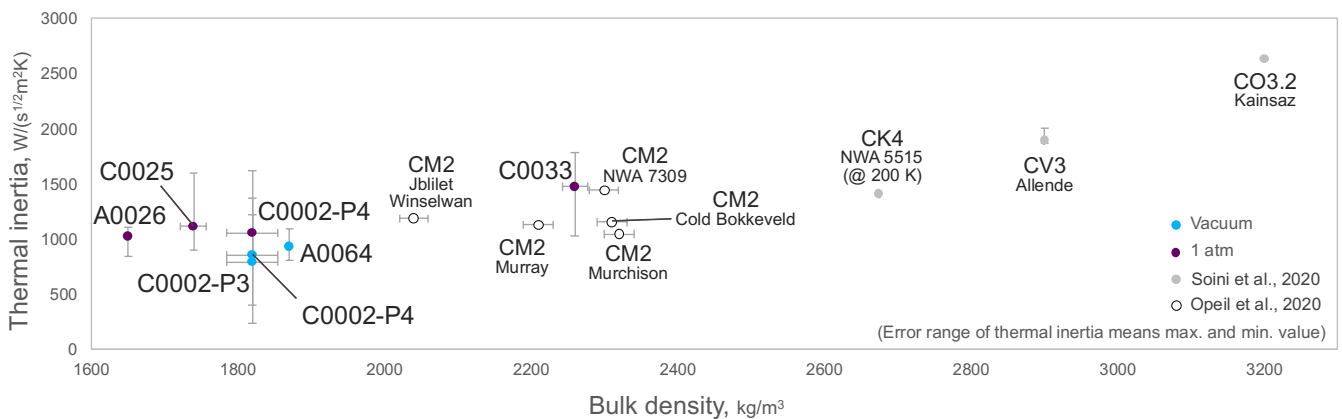


Figure 2. Thermal inertia vs. bulk density of Ryugu samples and carbonaceous chondrites.

## References

- [1] T. Yokoyama et al., Science abn7850 (2022). [2] K. Yomogida et al., J Geophys Res. 88 (1983) 9513–9533. [3] M. Beech et al., Planet Space Sci. 57 (2009) 764–770. [4] A.J. Soini, et al., Meteorit Planet Sci. 55 (2020) 402–425. [5] T. Ishizaki et al., Int J Thermophys. 43 (2022). [6] T. Nakamura et al., Science abn8671 (2022). [7] C. Opeil et al., Meteor Planet Sci. 55(8) (2020) E1–E20. [8] T. Okada et al., Nature. 579 (2020) 518–522.

# Thermal properties of asteroid Ryugu from global, local, and micro-scale observations and the possible formation and evolution scenario of Ryugu

Tatsuaki Okada<sup>1,2</sup>, Satoshi Tanaka<sup>1,2</sup>, Naoya Sakatani<sup>1</sup>, Yuri Shimaki<sup>1</sup>, Takehiko Arai<sup>3</sup>, Hiroki Senshu<sup>4</sup>, Hirohide Demura<sup>5</sup>, Tomohiko Sekiguchi<sup>6</sup>, Toru Kouyama<sup>7</sup>, Masanori Kanamaru<sup>2</sup>, Takuya Ishizaki<sup>1</sup>

<sup>1</sup>*Institute of Space and Astronautical Science, JAXA, Japan*, <sup>2</sup>*University of Tokyo, Japan*, <sup>3</sup>*Maebashi Institute of Technology, Japan*, <sup>4</sup>*Chiba Institute of Technology, Japan*, <sup>5</sup>*University of Aizu, Japan*, <sup>6</sup>*Hokkaido University of Education, Asahikawa, Japan*, <sup>7</sup>*National Institute of Advanced Industrial Science and Technology, Japan*..

Thermophysical properties of C-type asteroid 162173 Ryugu have been investigated through remote sensing using the Thermal Infrared Imager (TIR)[e.g., 1-3], on the surface using the radiometer MARA on MASCOT lander [4,5], and the analysis of return sample [e.g.,6,7]. The global average and the local distribution of thermal inertia were mapped by TIR, with the typical value of 200 to 400 J m<sup>-2</sup> kg<sup>-1</sup> s<sup>-0.5</sup> (tiu, hereafter) [1], which is lower than that of typical carbonaceous chondrite meteorites of 600 to 1000 tiu [8]. Surface boulders and their surroundings have almost the same thermal inertia, indicating that most of boulders are consisted of materials with high porosity (pores and cracks in them) and not completely consolidated, and the surroundings are covered with boulders and rocks (not sandy regolith) [1], which was confirmed during the descent operations. The flat diurnal temperature profiles observed at the afternoon local time indicate the very rough surface [1]. Considering the thermal model with rough surface [9], the thermal inertia and roughness are derived simultaneously [2]. Up-close observations by TIR during the descent operations suggested that boulders have a variety of thermal inertia, with more than 80 % of them having 200 to 400 tiu, while some portions have very low (<100 tiu) or very high (>600 tiu) thermal inertias [3]. They are identified as “Hot Spots” and “Cold Spots”, because they are observed exceptionally hotter or colder compared with their surroundings [1,3]. The surface experiment by MARA indicated the similar thermal inertia for a single boulder [4], so that the rough boulders should be the representative material on the asteroid. Multi-band radiometry by MARA indicates the similarity to aqueously altered carbonaceous chondrites (CI or CM) but not like heated carbonaceous chondrites [5].

The average thermal properties of returned samples show the thermal inertia almost similar to that of typical carbonaceous chondrites for <100 μm scale [6,7], although the thermal inertia (or more directly the thermal diffusivity) in the direction where cracks exist indicate much lower, consistent with the thermal inertia by remote sensing by TIR or surface measurements by MARA. The return samples are not always representative as the intact surface on Ryugu regarding the physical properties, since fragile portions of them might have been broken during impact sampling as well as during the severe shock and vibration in the return capsule when entry to Earth. The return samples seem to be consisted of more consolidated parts of Ryugu surface materials with flatter surface, instead of fragile and porous features observed as cauliflower-like crumbly boulders on Ryugu. The return samples are more like CI chondrites in mineralogy, chemistry, and textures but with darker, more porous and fragile characteristics [10,11]. The difference of thermal inertia between larger scale (> 1mm) and a smaller scale (<0.1 mm) might attribute to the existing cracks and pores inside of boulder materials. A formation scenario of Ryugu will be shown to explain the history of Ryugu formation and evolution or even a planetary formation.

Our scenario is like this: 1) porous dust with ices of volatile species (water and CO<sub>2</sub>) were accumulated to form a planetesimal in the outer solar system. 2) Aqueous alteration occurred by internal heating due to radioactivity of Al<sup>26</sup> but not heated to drive strong thermal metamorphism. Materials were more altered at the innermost region to consolidate almost equal to typical carbonaceous chondrites, but less altered at the outermost region to leave the materials so porous and fragile. 3) The parent body migrated to inner region of the Solar System, 4) Impact fragmentation of parent body, sometimes by S-type bodies [12]. 5) Degassing of volatiles by sublimation due to exposure to space, to make freeze-dry porous materials. 6) Reaccretion of fragmented rocks and boulders with high porosity by low degree of consolidation and freeze-dry and formation of a rubble pile body. Most of surface boulders are occupied by those from the inner region of the parent body as the representative boulders, while relatively porous boulders originated from the outermost region are the “hot spots” and relatively consolidated boulders originated from the innermost region are the “cold spots”. 7) Some uppermost surface processes by spaceweathering.

## References

- [1] Okada T. et al, 2020. *Nature* 579, 518-522. [2] Shimaki Y. et al., 2020. *Icarus* 348, 113835. [3] Sakatani N. et al. 2021. *Nature Astron.* 5, 766-774. [4] Grott M. et al. 2019. *Nature Astron.* 3, 971-976. [5] Hamm M. et al. 2022. *Nature Comm.* 13, 364. [6] Nakamura T. et al. 2022 *Science* abn8671. [7] Ishizaki T. et al. This issue, [8] Flynn, GJ, 2018. *Chem. Erde.* 78, 269-298. [9] Senshu H. et al. 2022. *Intl J. Thermophys.* 43, 102. [10] Yada T. et al. 2022. *Nature Astron.* 6 214-220. [11] Pilorget et al. 2022. *Nature Astron.* 6, 221-225. [12] Tatsumi E. et al. 2021. *Nature Astron.* 5, 39-45.

## Evidence of Permafrost Processes in C-asteroid Regoliths

M. Zolensky<sup>1</sup>, T. Nakamura<sup>2</sup>, T. Mikouchi<sup>3</sup>, H. Yurimoto<sup>4</sup>, T. Noguchi<sup>5</sup>, R. Okazaki<sup>6</sup>, H. Yabuta<sup>7</sup>, H. Naraoka<sup>6</sup>, K. Sakamoto<sup>8</sup>, S. Tachibana<sup>3</sup>, S. Watanabe<sup>9</sup>, and Y. Tsuda<sup>8</sup>

<sup>1</sup>ARES, NASA Johnson Space Center, Houston, TX 77058, USA ([michael.e.zolensky@nasa.gov](mailto:michael.e.zolensky@nasa.gov)); <sup>2</sup>Tohoku University, Miyagi 980-8578, Japan; <sup>3</sup>The University of Tokyo, Tokyo 113-0033, Japan; <sup>4</sup>Hokkaido University, Sapporo 060-0819, Japan; <sup>5</sup>Kyoto University, Kyoto 606-8502, Japan; <sup>6</sup>Kyushu University, Fukuoka 819-0395, Japan; <sup>7</sup>Hiroshima University, Higashi-Hiroshima 739-8526, Japan; <sup>8</sup>ISAS/JAXA, Sagami-hara 252-5210, Japan; <sup>9</sup>Nagoya University, Nagoya 467-8501, Japan.

**Introduction:** C-complex asteroids have suffered a wide variety of physical processing, some of which are not very obvious. Carbonaceous chondrites experienced and recorded a very wide range of chemical and physical processing in both nebular and asteroidal settings [1-7], resulting in the following textures: brecciation, flattened chondrules and foliation (CV and CM chondrites in particular), carbonate and phyllosilicate veins (CI, CM, CV3 dark inclusions), local alignment of matrix phyllosilicates (CR2, CI, CM), and shearing (mylonitization) around lithic fragments. Many of the extensively altered carbonaceous chondrites contain rounded to elliptical aggregates of phyllosilicates, carbonates, spinels (chromite and magnetite), Fe-Ni sulfides, and embayed olivines and pyroxenes, generally ascribed to impact shock or static burial pressures [6,7]. However, it is probable that even in the wettest regions of an asteroid dry periods were experienced during the periodic breaching of an icy surficial rind [8], which could have occurred during impacts or "volcanic" venting of gas and heat from the interior (this assumes internal heating). Thus, there should have been multiple wet-dry cycles experienced by these regolith or immediately subsurface materials. We have previously suggested that all the deformation features mentioned above would have arisen naturally from cycles of wet-dry and, more critically, freeze-thaw environmental conditions (permafrost) in asteroid regoliths [5]. Here we detail two related textures observed in CI chondrites, including asteroid Ryugu samples (essentially CI chondrite), consistent with permafrost processes.

**Permafrost Processes in Regoliths:** It is well-known to soil scientists that conditions of radically alternating humidity can have important morphologic and petrologic consequences [9]. Grains and lithic clasts can become rotated, crushed and drawn out into linear features (shearing). Porosity (including contraction and shearing cracks) and other bulk physical properties will vary in a dramatic manner. Easily altered materials will be dissolved while more resistant materials will be pulverized and mixed into matrix. These effects would be most pronounced for the C1-2 lithologies where the swelling clay saponite can be found in abundance, including the CI chondrite meteorites and asteroid Ryugu samples. Another important process to be considered is periodic growth and melting of ice crystals in the regolith [10-11]. The positive molal volume change during crystallization of water will induce oriented microfibrils to develop in the regolith, normal to the direction of ice crystal growth. Thus, masses of platy grains (in this case phyllosilicates, especially saponite flakes) will develop a pronounced compaction and preferred alignment. This process will recur for each freezing episode. Since the orientation of the growing ice mass will vary for each succeeding generation of growth, the eventual result will be to impart a particular, invasive, regolith fabric consisting of sheets of aligned clays for each generation, which will appear as anastomosing strings of phyllosilicates with roughly aligned basal directions in polished or thin sections (Figure 1). Our study has revealed that such textures are common in the CI chondrites.

Ice crystal growth could explain the preferred alignment of saponite observed in some Ryugu samples (see Figure 6b of [12]). However, a more likely explanation for this particular texture is mobilization of saponite flakes during wet, water saturated episodes, and deposition of these flakes onto the surface of underlying rock fragments under the force of gravity. These features are termed "silt caps", and these are a common feature of permafrost soils [11,13]. Of course, a major difference between permafrost processes on earth as compared to asteroids is the greatly reduced gravity on the latter. However, mass wasting is usually observed on small bodies including asteroids (including Ryugu and Bennu) and comet nuclei [14,15], so gravity-driven processes operated on the Ryugu parent body. Growth and collapse of subsurface asteroidal icicles would also impart cyclical changes in bulk regolith porosity, induce rotation and movement of crystals and lithic fragments through frost heaving, and consequent shearing [11]. This process could also account, to some degree, for the flattened chondrules observed in some carbonaceous chondrites (especially CMs).

**Conclusions:** We therefore suggest that cyclical, indigenous environmental processes, rather than impact gardening, could be responsible for some of the late-stage petrologic characteristics of wet carbonaceous chondrites, and Ryugu samples. We note that this suggestion has also recently been proposed by another group [16]. Bulk petrographic features of additional Ryugu samples and carbonaceous chondrites should be investigated more systematically in order to test this idea, especially samples rich in clays such as saponite.

**References:** [1] Moskovitz et al. (2013) *Icarus* **224**, 24; [2] Vilas (2008) *Ap. J.* **135**, 1101–1105; [3] Lazaro et al. (2012) *A&A* **549**, L2; [4] Zolensky et al. (2022) *MAPS* **57**, MAPS.13909; [5] Zolensky (1995) *Meteoritics* **30**, 606-607; [6] Sneyd et al. (1988) *Meteoritics* **23**, 139-149; [7] Scott et al. (1992) *GCA* **56**, 4281-4293; [8] DuFresne and Anders (1962) *GCA* **26**, 1085-1114; [9] Nahon (1991) *Introduction to the Petrology of Soils and Chemical Weathering*, pp. 122-133; [10] Van Vliet and Fox (2018) Frost Action. In *Interpretation of Micromorphological Features of Soils and Regoliths, 2nd Ed.*, Elsevier; [11] Zhang et al. (2021) The Influence Mechanism of Freeze-Thaw on Soil Erosion: A Review. *Water* **13**, 1010; [12] Nakamura T. et al., (2022) *Science* **377**, 10.1126/science.abn8671; [13] Menzies and Ellwanger (2011) *Boreas* **40**, 271-288; [14] Jawin et al.

(2020) *JGR Planets* **125**, Issue 8; [15] Steckloff and Samarasinha (2018) *Icarus* **312**, 172-180; [16] Nakamura E. et al. (2022) *Proceedings of the Japan Academy, Series B* **98**, 227-282.

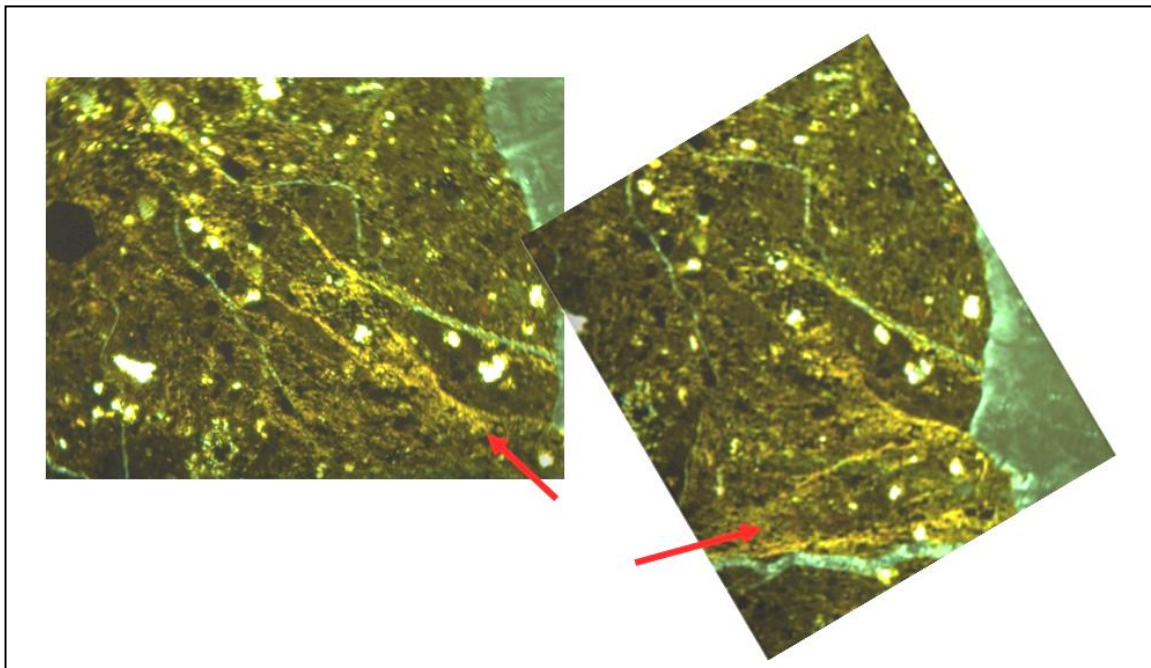


Figure 1. Ivuna CI chondrite, in cross polars. Two views of the same area in different rotation angles showing two distinct directions of phyllosilicate (yellow stringers) preferential orientations (arrows). Views measure 2 mm in longest dimension.

## Modeling of aqueous alteration in the parent body of the asteroid Ryugu

A. Tsuchiyama<sup>1,2</sup>, J. Matsuno<sup>1</sup> and M. Matsumoto<sup>3</sup>

<sup>1</sup> Research Organization of Science and Technology, <sup>2</sup>CAS, Guangzhou Institute of Geochemistry, <sup>3</sup>Tohoku University

The mineralogy, petrology and chemical properties of the samples collected from the asteroid 162173 Ryugu by the Hayabusa2 spacecraft show that the samples correspond to CI meteorites not affected by terrestrial weathering (e.g., [1-3]). The parent body of Ryugu were formed by accretion of minerals, organics, and ice, and aqueous alteration occurred by reaction of melted ice with the minerals and organics [1]. The major lithology of the Ryugu samples consists mostly of hydrous phyllosilicates (serpentine and saponite), carbonates, FeS and magnetite which precipitated from liquid (melted ice) during the aqueous alteration. Least- and less-altered lithologies, where some anhydrous minerals, such as olivine, remained unaltered or partially altered, were also observed [1]. Model chemical equilibrium of the aqueous alteration was calculated in an appropriate condition (e.g., 40°C based on oxygen isotope equilibrium [2] and ice of H<sub>2</sub>O + 0.08 CO<sub>2</sub> based on CO<sub>2</sub>-bearing fluid inclusion[1]) as a function of the initial water/rock ratio (in mass),  $W/R$ , and found that the mineral assemblages are almost consistent with the least-altered, less-altered and altered major lithologies at  $W/R$  of 0.06 to 0.1, 0.1 to 0.2, and 0.2 to 0.9, respectively [1]. The order of precipitation of minerals in the major lithology was also estimated from the included and enclosed relations among these minerals [4].

We understood the outline of the aqueous alteration by the Ryugu sample initial analysis as mentioned above. However, we still do not know how the aqueous alteration occurred and ceased; for example, how liquid was present, and precipitation occurred from the liquid. Therefore, in this study, we performed a modeling of the aqueous alteration by reference to the minerals and their assemblages and the chemical composition of the Ryugu samples.

In the present model, we made the following assumptions to simplify the problem; (1) the system Mg-Fe-Si-Ca-O-S-C-H is taken into consideration with the bulk chemical composition of CI [5] that is unchanged during the alteration except for O (oxidation or reduction permitted). (2) The starting material is composed of anhydrous minerals, amorphous silicate, organics, and CO<sub>2</sub>-H<sub>2</sub>O ice. Olivine, metallic Fe, and FeS are considered for the anhydrous minerals. We adopted Mg# (Mg/(Mg+Fe) in mole) of 0.99 for olivine, which was observed in least- and less-altered lithologies [6]. Material similar to GEMS (glass embedded with metal and sulfide) is considered for amorphous silicate based on the observation in the least-altered lithology [1]. This GEMS-like material (GLM) is assumed to have the mean GEMS composition of [7]. We consider relatively oxidized GLM, where only nanoFeS particles (without nanoFe) are embedded in FeO-bearing amorphous silicate. Thus, the Mg# of the amorphous silicate becomes 0.612 to maintain the mean GEMS composition. The density of GLM is assumed to be 3 g/cm<sup>3</sup>. (3) We consider only IOM as organics. The chemical composition of IOM is adopted from [8] and its density is assumed to be 1.3 g/cm<sup>3</sup>. IOM is not changed by the alteration. (4) The ice CO<sub>2</sub>/H<sub>2</sub>O ratio is 0.08 as proposed by [1]. The ice melts to form CO<sub>2</sub>-bearing water. The temperature is 40°C proposed by [2] and the pressure is less than ~50 bar for a 50-km-radius parent body [1]. In these conditions, the melted ice is a liquid state (not fluid) and the densities of H<sub>2</sub>O and CO<sub>2</sub> are almost constant (1 g/cm<sup>3</sup> [9] and 1.04 g/cm<sup>3</sup> [10], respectively). (5) The aqueously altered products are serpentine, saponite, FeS, magnetite, and dolomite. The Mg#'s of serpentine and saponite are 0.85 based on the Ryugu sample analysis [1]. Dolomite is only considered as a carbonate although other carbonates (magnesite and calcite) are present in the Ryugu samples. (6) GLM starts to react with liquid to form serpentine and saponite first, and simultaneously the same proportion of Fe as that of altered GLM becomes magnetite. If the GLM is completely altered, olivine starts to react with liquid. (7) GLMs and the phyllosilicates (serpentine and saponite) have nano-sized pores (nanopores) based on the TEM observation of the Ryugu samples [1]. Any other pores are not present in the initial state, but the space that used be as ice acts as micron-sized pores (micropores). (8) The water/rock ratio,  $W/R$ , is defined as the mass ratio of water (or ice) to whole of the other materials including IOM.

The amounts of the formula weights of the phases (minerals, IOM and liquid) were calculated to have elemental balance among the chemical compositions of the phases and the bulk chemical compositions, and their volumes were obtained from the densities of the phases. This calculation is similar to the CIPW norm calculation, and chemical equilibrium was not considered. We made calculation for a case where the initial IOM volume is 10% with respect to solid phases and the porosities of the nanopores in both GLM and phyllosilicates are 40%.

In the initial state, the modes of olivine, Fe, FeS (nanoFeS in GLM not included), GLM with nanopores, and IOM are calculated to be 17.2, 2.5, 4.9, 67.4, and 8.1 vol.%, respectively, to have the elementary balance (Fig.1 at  $W/R = 0$ ). We changed the initial water/rock ratio (in mass),  $W/R$ , as a parameter. The final mineral assemblages after the complete reaction with liquid were calculated with different  $W/R$ . Changes in the volumes of the phases are shown in Fig. 1. In the range of  $W/R = 0$  to 0.10 (Stage-1 in Fig. 1), mainly saponite and minor amounts of serpentine and magnetite form from GLM and Fe, and H<sub>2</sub>O in liquid

is completely consumed. CO<sub>2</sub> in liquid is also completely consumed to form dolomite, and therefore no liquid remains in this stage after the aqueous alteration. GLM and Fe are completely consumed at  $W/R = 0.10$ . With further increase in  $W/R$ , olivine starts to react with water, and serpentine forms by consuming some saponite together with olivine to accommodate their Mg/Si ratios ( $W/R = 0.10$  to  $0.12$ , Stage-2 in Fig. 1). Olivine is completely consumed at  $W/R = 0.12$ , and no liquid remains in this stage too. In  $W/R > 0.12$ , some liquid remains after complete reaction with GLM, Fe and olivine, and the volumes of magnetite, saponite, serpentine, and FeS are constant ( $W/R = 0.12$  to  $0.19$ , Stage-3 in Fig. 1). The volume of dolomite increases by consuming CO<sub>2</sub> in liquid, and no CO<sub>2</sub> remains in liquid in this stage. In  $W/R > 0.19$  (Stage-4 in Fig. 1), some CO<sub>2</sub> remains in liquid because  $[C] > 2[Ca]$  and the volume of dolomite is constant. Stage-1, Stage-2 and Stages-3 and -4 roughly correspond the least-altered, less-altered, and altered major lithologies, respectively, in terms of their mineral assemblages. The modes of dolomite, magnetite, saponite with nanopores, serpentine with nanopore, FeS, and IOM in Stage-4 are 2.0, 4.3, 31.3, 48.1, 8.1, and 6.2 vol.%, respectively. These are similar to those of the main lithology [1]. The relation of  $W/R$  and stages are also roughly consistent with the chemical equilibrium calculation of [1]. The boundary between Stages-2 and -3 ( $W/R = 0.12$ ) corresponds to  $W/R = 0.18$  in [1]. This difference is derived from the rough calculation in the present model. The broad similarities suggest that the present model roughly reflects the equilibrium although the model itself does not consider equilibrium.

As a next step, we calculated the proportions of liquid filling pores. The total volume of the bulk material consisting of minerals, IOM, and pores (nanopore in GLM and/or phyllosilicates and micropore after ice) increases by the aqueous alteration from the initial volume (minerals, IOM, nanopore in GLM, and ice) by  $\sim 10 - 20\%$ . Because such volume increase would not occur for asteroids, we assumed that the initial bulk volume maintains constant by collapsing some of micropores. Liquid (if present) occupies the remaining pores. Fig. 2 shows the liquid proportion filling pores,  $f$ , and the total porosity including liquid,  $\phi$ , as a function of  $W/R$  for the initial state before aqueous alteration. As we assumed liquid preferentially fills nanopores due to capillarity, with increasing  $W/R$ ,  $f(\text{nanopore})$  increases first, and then  $f(\text{micropore})$  increases after  $f(\text{nanopore})$  reaches 100%. For the final state after aqueous alteration (Fig. 3), similar behavior of  $f$ 's can be seen, but  $f(\text{nanopore})$  and  $f(\text{micropore})$  are 0% in Stages-1, and -2. These results showed that liquid partially occupies only nanopores if  $W/R$  is small, and even if  $W/R$  is large, macropores are not fully filled with liquid, suggesting that pores are not fully filled with liquid during aqueous alteration. The bulk density of Ryugu samples was determined to be  $1.79 \text{ g/cm}^3$ , indicating the porosity of 31% if we compared with the grain density of CI meteorites [1]. If the porosity has not changed from the end of aqueous alteration to present,  $\phi$  of 31% corresponds to  $W/R$  of 0.19 (Fig. 3), where 100% of nanopores and 61% of micropores are filled with liquid, respectively, before the alteration (Fig. 2), and 55% of nanopores and 0% of micropores are filled with liquid, respectively, after the alteration (Fig. 3). These suggest that aqueous alteration in the Ryugu parent body should occur through dissolution and reprecipitation in conditions where not so much water present.

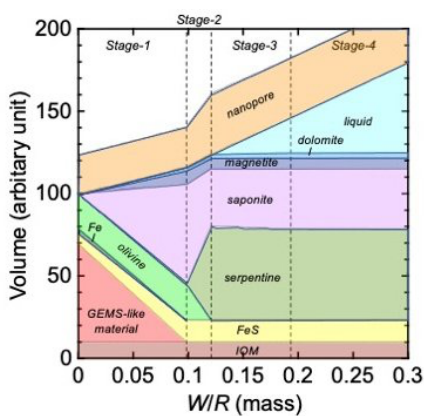


Figure 1. The volumes of phases after aqueous alteration at different water/rock ratio,  $W/R$ .

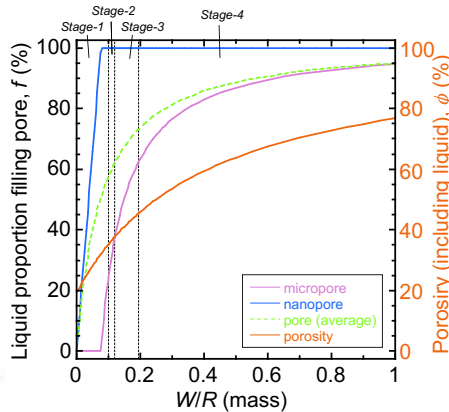


Figure 2. Liquid proportion filling pores and porosity before aqueous alteration.

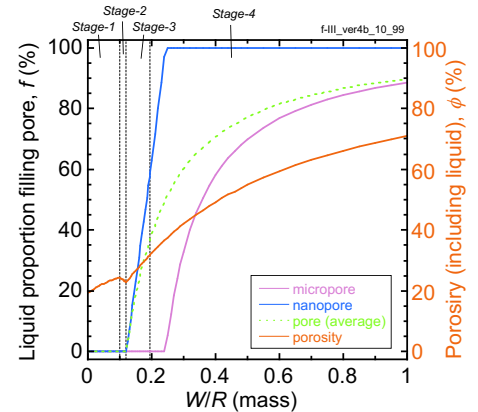


Figure 3. Liquid proportion filling pores and porosity after aqueous alteration.

## References

- [1] Nakamura T. et al. 2022. Science. 10.1126/science.abn8671. [2] Yokoyama T. et al. 2022. Science 10.1126/science.abn7850. [3] Ito M. et al. 2022. Nature Astron. 10.1038/s41550-022-01745-5. [4] Tsuchiyama A. et al. 2022. 85th Annual Meeting of The Meteoritical Society 2022 6221.pdf. [5] Lodders K. et al. 2009. Landolt–Bornstein (Berlin: Springer), 42. [6] Mikouchi T. et al. 2022. 85th Annual Meeting of The Meteoritical Society 2022 6180.pdf. [7] Keller L.P. and Messenger S. 2011. Geochim. Cosmochim. Acta 75:5336. [8] Alexander C.M.O'D. et al. 2007. Geochim. Cosmochim. Acta 71:4380. [9] Xiaoyan Ji. et al. 2005. Ind. Eng. Chem. Res. 44:8419. [10] Longhi J. et al. 2005. Geochim. Cosmochim. Acta 6: 529.

## Chemical abundances in Ryugu, nugget effect, and cosmic composition

Nicolas Dauphas<sup>1</sup>, Tetsuya Yokoyama<sup>2</sup>, Ryota Fukai<sup>3</sup>, Tomohiro Usui<sup>3</sup>, Shogo Tachibana<sup>4</sup>, Maria Schönbächler<sup>5</sup>, Andrew M. Davis<sup>1</sup>, Hisayoshi Yurimoto<sup>6</sup>, The Hayabusa2-initial-analysis chemistry team, The Hayabusa2-initial-analysis core.

<sup>1</sup>*Origins Lab, Dept. of the Geophysical Sciences and Enrico Fermi Institute, The University of Chicago, USA*

<sup>2</sup>*Dept. of Earth & Planetary Sciences, Tokyo Institute of Technology, Japan*

<sup>3</sup>*Dept. of Solar System Sciences, ISAS, JAXA*

<sup>4</sup>*Dept. of Earth and Planetary Science, University of Tokyo, Japan*

<sup>5</sup>*Inst. für Geochemie und Petrologie, ETH Zürich, Switzerland*

<sup>6</sup>*Dept. of Earth and Planetary Sciences, Hokkaido University, Japan*

Approximately 99.86% of the mass of the solar system is locked up in the Sun, which is largely inaccessible and whose composition is only known through spectroscopy and analysis of solar wind. Much of our knowledge of the chemical and isotopic compositions of the bulk solar system comes from analysis of meteorites, and among those CI (Ivuna-type) carbonaceous chondrites, which contain most elements except the most volatile ones in proportions that match estimates from solar photosphere observations [1,2]. CI chondrites are rare and most of them have been in meteorite collections for many decades (the largest one, Orgueil, fell in 1864), where they have been exposed to moisture, airborne and handling contaminants. The Hayabusa2 mission sampled ~5.4 g of pristine material from Ryugu, a Cb-type asteroid [3]. Laboratory analyses of the returned sample show that Ryugu is related to CI chondrites and probably originated from the outskirts of the solar system [4-7]. The only known contaminant for Ryugu samples is Ta in the projectile used to liberate dust and fragments from Ryugu's surface [8]. Given their pristine nature, Ryugu samples are ideally suited to constrain the composition of outer-solar system material, which we take as a proxy for the solar composition. A caveat to estimating the solar composition using Ryugu or CI chondrites is that these may contain extraneous refractory dust compared to other inner solar system objects. This was most clearly demonstrated with rare earth elements (REEs), as carbonaceous chondrites all show Tm anomalies relative to non-carbonaceous chondrites [9,10], presumably due to the presence of refractory dust with a group II REE pattern characterized by large positive Tm anomalies produced by evaporation/condensation processes in the solar nebula [11]. At this stage, it is unclear if the Sun would contain the same complement of refractory dust as CI chondrites, or if inner solar system objects are more representative.

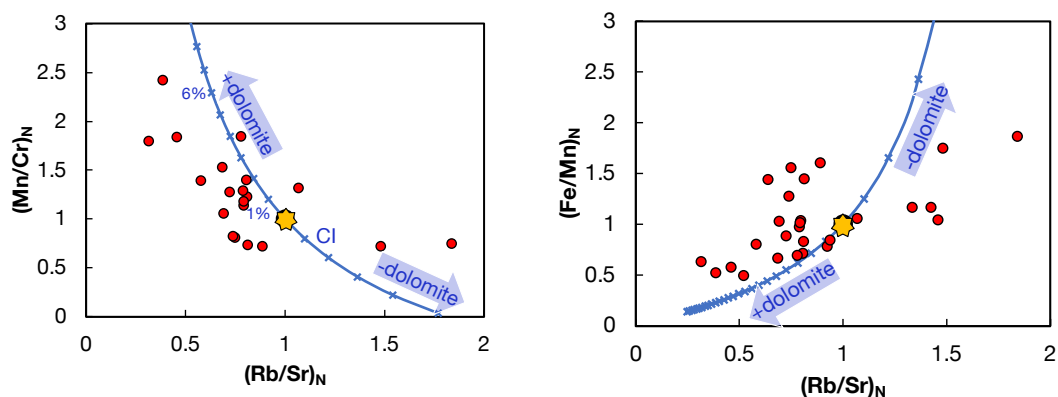


**Fig. 1.** Correlations between Mn/Cr, Fe/Mn, and Rb/Sr ratios. The yellow star is the CI composition. The red points are bulk fragment measurements for Ryugu [4,7]. The curves are calculated mixing curves between bulk CI and dolomite in CI chondrites [12,13].

Yokoyama *et al.* [4] and Nakamura E. *et al.* [7] reported high precision chemical composition analyses of Ryugu fragments by quadrupole inductively coupled plasma mass spectrometry (Q-ICP-MS), the gold standard for such analyses. Those measurements show that Ryugu has almost unfractionated chemical abundances relative to CI chondrites, strengthening the case for a link between Cb-asteroid and CI chondrites. The fragments analyzed are relatively small (from ~0.2 to ~30 mg) and show significant departures relative to CI chondrites that are unrelated to volatility. This is true even in the largest fragments analyzed, which show significant enrichments in REEs, Ca, Sr, Ba, P, and Mn [4]. Chemical abundance variations have been seen previously in chondrites that presumably reflect heterogeneous distribution (and unrepresentative sampling) of phases highly enriched in some elements [9]. This is known as a nugget effect and represents a limit in the precision that can be attained in bulk rock analyses. Carbonate and phosphate phases have been found in Ryugu samples [4,6,7] and could be responsible for the chemical variations seen in bulk fragment analyses.

A nugget effect for REEs associated with the presence of phosphate was identified in carbonaceous and ordinary chondrites [9]. There are several telltale signatures of such a nugget effect. The first one is that in elemental ratio plots, "bulk" analyses should define mixing curves between the true bulk and the mineral composition. In ordinary and carbonaceous chondrites, the presence of phosphate nuggets was identified as a negative correlation between La/Lu ratios and Eu/Eu\* (=observed Eu/interpolated Eu) anomalies (phosphates in ordinary chondrites have high La/Lu and negative Eu/Eu\* anomalies) [9]. The phosphates in Ryugu lack these characteristic features and are more difficult to detect [7]. Ryugu fragments are rich in dolomite, which has high Mn/Cr, low Rb/Sr, and low Fe/Mn. In Fig. 1, we plot CI-normalized Mn/Cr and Fe/Mn against Rb/Sr. As shown, the ratios are correlated, and the variations observed can be well explained by admixture or removal of dolomite at the percent level. Another telltale signature of a nugget effect is that the dispersion in elemental ratios should decrease as the inverse of the square root of the mass of sample homogenized [9]. As shown in Fig. 2, the dispersions in elemental ratios are consistent with a sampling problem associated with a nugget effect. The dispersion in elemental ratios can be calculated if the nugget size, abundance, and composition are known [9]. Because these are poorly constrained for carbonates, we calculated instead the dispersion for the smaller fragments digested and calculated the predicted dispersion for larger masses. Having established that unrepresentative sampling of carbonate is likely responsible for the dispersion in specific elemental ratios, we can predict the expected dispersion if large sample masses are digested. We thus estimate that for 1 g of Ryugu sample homogenized/digested, the dispersion ( $2\sigma$ ) of the bulk Mn/Cr and Rb/Sr ratios will be better than  $\sim\pm 5\%$ . Elements that are not concentrated in specific minerals will be much less affected by this uncertainty. Our analysis shows that much of the dispersion in chemical composition between Ryugu grains is a due to non-representative sampling of mineral phases highly enriched in some elements. This artifact can be remediated by homogenizing a larger sample mass ( $\sim 1$  g), which is important to constrain the "cosmic" composition, and test if previous estimates based on CI chondrites are reliable.

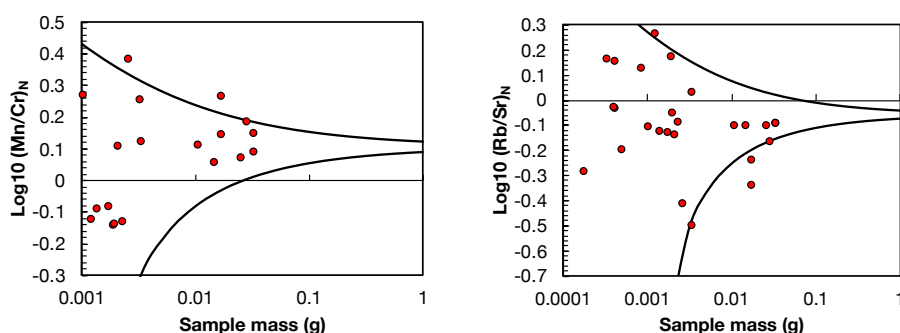


**Fig. 2.** Elemental ratios sensitive to carbonate nugget effects against mass homogenized/digested. If a nugget effect is present, we would expect the dispersion to decrease as the inverse of the square root of the mass of sample homogenized/digested (black envelope) [9]. As shown, this seems to be the case.

**References.** [1] Lodders, K., 2021. *Space Science Reviews*, 217, 1. [2] Asplund M. et al. 2021. *Astronomy & Astrophysics* 653, A141. [3] Yada T. et al. 2022. *Nature Astronomy* 6:214. [4] Yokoyama T. et al. 2022 *Science* eabn7850. [5] Ito, M et al. 2022. *Nature Astronomy*, 1, <https://doi.org/10.1038/s41550-022-01745-5>. [6] Nakamura T. et al., 2022. *Science*, eabn8671. [7] Nakamura E. et al. (2022) *Proceedings of the Japan Academy, Series B* 98, 227. [8] Sawada H. et al. 2017. *Space Science Reviews*, 208, 81. [9] Dauphas, N. and Pourmand, A., 2015. *Geochimica et Cosmochimica Acta*, 163, 234. [10] Barrat, J.A., Dauphas, N., et al., 2016. *Geochimica et Cosmochimica Acta*, 176, 1. [11] Hu, J. Y., et al. (2021). *Science Advances*, 7(2), eabc2962. [12] Endreß, M. and Bischoff, A., 1996. *Geochimica et Cosmochimica Acta* 60, 489. [13] Macdougall, J.D., et al. 1984. *Nature*, 307, 249.

**The Hayabusa2-initial-analysis chemistry team:** T. Yokoyama, K. Nagashima, I. Nakai, E.D. Young, Y. Abe, J. Aléon, C.M.O'D. Alexander, S. Amari, Y. Amelin, K. Bajo, M. Bizzarro, A. Bouvier, R. W. Carlson, M. Chaussidon, B.-G. Choi, N. Dauphas, A. M. Davis, T. Di Rocco, W. Fujiya, R. Fukai, I. Gautam, M. K. Haba, Y. Hibiya, H. Hidaka, H. Homma, P. Hoppe, G.R. Huss, K. Ichida, T. Iizuka, T.R. Ireland, A. Ishikawa, M. Ito, S. Itoh, N. Kawasaki, N. T. Kita, K. Kitajima, T. Kleine, S. Komatani, A. N. Krot, M.-C. Liu, Yuki Masuda, K.D. McKeegan, M. Morita, K. Motomura, F. Moynier, A. Nguyen, L. Nittler, M. Onose, A. Pack, C. Park, L. Piani, L. Qin, S.S. Russell, N. Sakamoto, M. Schönbächler, L. Tafla, H. Tang, K. Terada, Y. Terada, T. Usui, S. Wada, M. Wadhwa, R.J. Walker, K. Yamashita, Q.-Z. Yin, S. Yoneda, H. Yui, A.-C. Zhang, H. Yurimoto.

**The Hayabusa2-initial-analysis core:** S. Tachibana, T. Nakamura, H. Naraoka, T. Noguchi, R. Okazaki, K. Sakamoto, H. Yabuta, H. Yurimoto, Y. Tsuda, S. Watanabe.

## Abundance and properties of Ryugu diffuse organic matter

Rhonda Stroud<sup>1,2</sup>, Bradley De Gregorio<sup>2</sup>, Jens Barosch<sup>3</sup>, Larry Nittler<sup>1,3</sup>

The Hayabusa2-initial-analysis Organic Macromolecule Team and Core Team

<sup>1</sup>*School of Earth and Space Exploration, Arizona State University, USA,*

<sup>2</sup>*Materials Science and Technology Division, US Naval Research Laboratory, USA,*

<sup>3</sup>*Earth and Planets Laboratory, Carnegie Institution of Washington, USA*

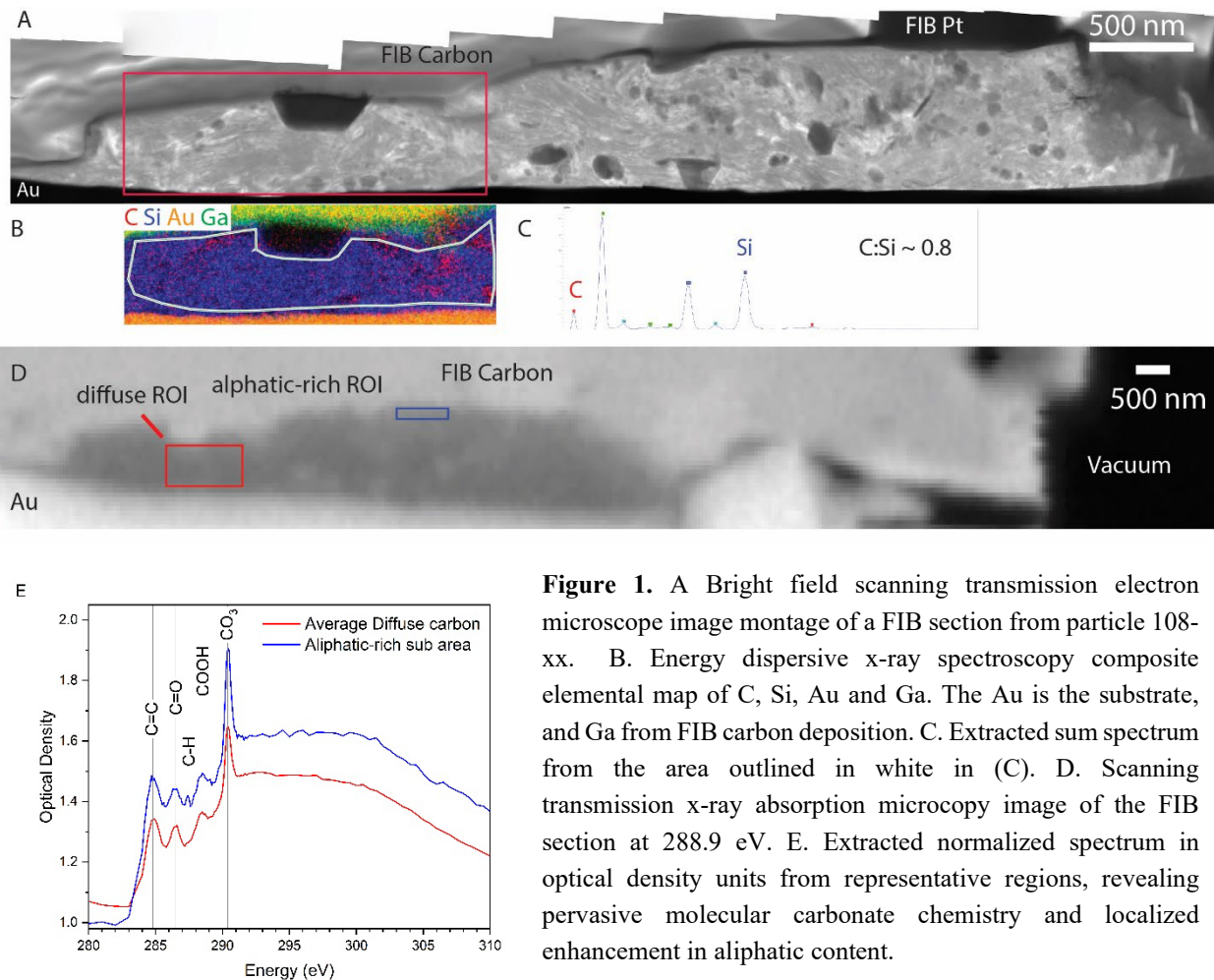
Initial Analysis studies have revealed that Ryugu regolith particles contain abundant organic carbon (3 wt%) [1,2], and that organic matter has the same range of morphologies as previously observed in primitive chondrites, including solid and hollow nanoglobules, nanodiamonds, dense, irregularly shaped particles, and diffuse materials with poorly-defined boundaries [3]. The diffuse organics form coatings on and fill the space between mineral grains, and intercalate into phyllosilicates. Because the diffuse carbon can be very thin (single nm) and intimately mixed with the nanoscale minerals, especially phyllosilicates, it is below the spatial limit for many techniques. Many analyses focus instead on globules or other organic particles > 200 nm. However, the diffuse carbon represents a substantial portion, possibly 50% or more, of the total organic carbon, and must be considered for a complete understanding of the Ryugu organics. To better understand the abundance and properties of diffuse carbon, we used correlated scanning transmission x-ray microscopy (STXM), scanning transmission electron microscopy (STEM) and nanoscale secondary ion mass spectrometry (NanoSIMS) to examine samples from Chambers A and B.

Figure 1A shows a bright-field STEM image montage of a focused ion beam (FIB) lift-out section from particle A108-?? pressed into a Au mount for NanoSIMS analysis. The BF STEM image shows a mixture sulfides and phyllosilicates with domain sizes of 10s to 100s of nm, but no discernable carbonaceous particles. However, STEM-based energy dispersive x-ray spectroscopy (EDS) mapping of the section Fig. 1B reveals carbon distributed throughout. Quantification of the C:Si molar ratio with Cliff-Lorimer routines for areas > 1 $\mu$ m<sup>2</sup> for no visible nanoglobules indicate values of  $\sim 0.8 \pm 0.3$ . Similar STEM-EDS analysis of additional FIB sections shows comparable C:Si ratios, confirming that a large portion of the organic carbon is present as diffuse matter rather than globular carbon in general, not only in this specific particle. However, it is difficult to obtain a precise determination of fraction of the diffuse vs. particulate carbon because the ability to resolve individual organic carbon particles < 100 nm depends greatly on the sample preparation and analysis conditions. In 100-nm thick FIB sections such as this, amorphous carbon particles as large as 50 nm could be hidden in images by the greater intensity variation of the phyllosilicates and sulfides, and only revealed by spectroscopy.

Measurement of the carbon K edge x-ray absorption near edge structure (XANES) with STXM can provide the average functional chemistry distribution of the diffuse carbon (Fig. 1D, Fig. 1E). Notably, there are four prominent peaks in the diffuse carbon spectrum from regions across this FIB section, with the typical aromatic (C=C), ketone (C=O), carboxyl (COOH) groups commonly seen in chondritic IOM, plus the CO<sub>3</sub> carbonate peak. Although the carbonate peak is very intense, the additional x-ray absorption peaks associated with crystalline carbonates are absent. In addition, the STEM-EDS shows Ca is absent, and no signs of Fe or Mg carbonate nanocrystals are observed in the STEM images. XANES spectra extracted from smaller ROIs show variability in the relative intensity of the four functional groups and in some cases distinct aliphatic-rich regions can be found (Fig. 1D blue box, 1E blue spectrum).

To better constrain the nature of the diffuse carbon, it is also helpful to analyze samples of particle prepared by ultramicrotome and as demineralized acid-insoluble organic matter (IOM) isolates. Those data are discussed but not shown here due to space constraints, but will be presented at the meeting. Some, but not all, of the diffuse organic matter is preserved in the IOM samples, and comprises the fine-grained porous material referred to as “fluffy”, distinct from the nanoglobules. Notably, the prominent carbonate peak, easily observed in the FIB sections, is not present in the IOM XANES data. The CO<sub>3</sub> peak is present though difficult to measure in the XANES data from microtomed

particles. Electron energy loss spectroscopy in the STEM, coupled with EDS, shows the carbonate peak is associated with organic carbon in direct contact with phyllosilicates. This suggests that different portions of the diffuse IOM have distinct chemical origins, with the molecular carbonate signature possibly due to reaction of C-rich fluids with phyllosilicates.



## References

[1] Yokoyama T et al. 2022. Science abn7850. [2] Yabuta H. et al. 2022. Abstract #2241. 53d LPSC. [3] Stroud R. M., et al. 2022. Abstract #2052. 53d LPSC.

**The Hayabusa2-initial-analysis Organic Macromolecule Team and Core Team:** H. Yabuta, G. D. Cody, C. Engrand, Y. Kebukawa, B. De Gregorio, L. Bonal, L. Remusat, R. Stroud, E. Quirico, L. R. Nittler, M. Hashiguchi, M. Komatsu, E. Dartois, J. Mathurin, J. Duprat, T. Okumura, Y. Takahashi, Y. Takeichi, D. Kilcoyne, S. Yamashita, A. Dazzi, A. Deniset-Besseau, S. Sandford, Z. Martins, Y. Tamenori, T. Ohigashi, H. Suga, D. Wakabayashi, M. Verdier-Paoletti, S. Mostefaoui, G. Montagnac, J. Barosch, K. Kamide, M. Shigenaka, L. Bejach, T. Noguchi, H. Yurimoto, T. Nakamura, R. Okazaki, H. Naraka, K. Sakamoto, S. Tachibana, S. Watanabe, and Y. Tsuda

# Sulfur-XANES of intact Ryugu grains and the isolated IOM

H. Suga<sup>1</sup>, Y. Tamenori<sup>1</sup>, H. Yabuta<sup>2</sup>, H. Yurimoto<sup>3</sup>, T. Nakamura<sup>4</sup>, T. Noguchi<sup>5</sup>, R. Okazaki<sup>6</sup>, H. Naraoka<sup>6</sup>, K. Sakamoto<sup>7</sup>, S. Tachibana<sup>8</sup>, S. Watanabe<sup>9</sup>, Y. Tsuda<sup>7</sup>, and the Hayabusa2-initial-analysis IOM team

<sup>1</sup>Japan Synchrotron Radiation Research Institute (JASRI/SPring-8), 1-1-1 Kouto, Sayo, Hyogo pref. 679-5198 Japan, <sup>2</sup>Hiroshima University, Japan, <sup>3</sup>Hokkaido University, Japan, <sup>4</sup>Tohoku University, Japan, <sup>5</sup>Kyoto University, Japan, <sup>6</sup>Kyushu University, Japan, <sup>7</sup>JAXA, Japan, <sup>8</sup>Univ. of Tokyo, Japan, <sup>9</sup>Nagoya University, Japan.

**Introduction:** The Hayabusa 2 spacecraft was launched on December 2014 to collect samples of the near-Earth C-type (carbonaceous) asteroid (162173) Ryugu [1]. This mission aims to investigate the origin and evolution of the early Solar System and life. In December 2020, the spacecraft returned 5.42 g of the Ryugu surface samples to the Earth [2]. The initial sample analysis team and the JAXA phase2 curation found that the elemental compositions, mineralogy, and organic chemistry of asteroid Ryugu were identical to those of CI chondrites [e.g., 3-6].

A variety of sulfur-bearing organic molecules have been identified from both soluble organic matter (SOM) and insoluble organic matter (IOM) in carbonaceous chondrites [e.g., 7-9]. Sulfur has a wide range in oxidation states from -2 to +6, so it can be used as a cosmochemical indicator of redox conditions; therefore, it contributes to elucidating the formation of organic molecules in the early Solar System. X-ray Absorption Near Edge Structure of Sulfur (S-XANES) can be used to estimate oxidation states of sulfur from a large chemical shift, and the chemical species can be discussed by the spectral profile. In this study, we conducted the S-XANES analysis on intact Ryugu grains and the isolated IOM to determine the sulfur composition.

**Samples and Method:** The Ryugu aggregate samples A0109-21 and C0057-1&2 were selected for S-XANES measurements. The acid treatment protocol of IOM isolation is described in [3] in detail. The intact Ryugu grains and the isolated IOM were analyzed by non-destructive bulk S K-edge XANES analysis at BL27SU in SPring-8.

**Results and Discussion:** Sulfur-XANES spectra were obtained from the intact Ryugu grains and the isolated IOM. The spectral profile of the intact grains is composed of the dominant peak around 2470.4 eV and broad spectra ranging from 2475.0 to 2484.0 eV. The peak of 2470.4 eV corresponds to the inorganic sulfide ( $S^{1-}$ ) [8]. Compared with the spectral profile of standard materials in the previous study [e.g., 10], it corresponds to pyrrhotite, a common sulfide in Ryugu [5]. In addition, a peak derived from sulfate ( $S^{6+}$ ) was observed at 2482.6 eV from A0109-21.

The S-XANES spectra of Ryugu IOM were entirely different from those of the intact grains. The peak around 2472.0 eV corresponding to organic sulfides (C-S-S-C, C-S-C) was the most prominent from the spectra of Ryugu IOM. The shoulder feature at 2474.3 eV is consistent with the presence of heterocyclic sulfur ( $S^0$ ) [9]. The broad profile ranging at 2477.0–2484.0 eV could be a mixture composed of oxidized organic sulfur species; such as sulfonate (R-SO<sub>2</sub>O-R'), sulfone (R-SO<sub>2</sub>-R'), and sulfites (R-SO<sub>3</sub>) [8]. A moderate peak of sulfates was also observed, which is likely to be correspond to organic sulfate (R-O-SO<sub>3</sub>) because inorganic sulfate compounds should have already been dissolved from the Ryugu samples during acid treatment to extract IOMs. No significant difference was found between IOMs extracted from A0109 and C0057.

The spectral shapes of the isolated Ryugu IOM were broadly similar to those of IOM from carbonaceous chondrites [8,9], except that the peak derived from inorganic sulfide was not detected from the Ryugu IOM. In particular, moderate abundances of heterocyclic sulfur and oxidized organic sulfur functional groups in Ryugu IOM were closer to those in IOM isolated from CM rather than that of CI. CI experienced a higher temperature (100–150 °C) than CM, and heterocyclic sulfur and oxidized organic sulfurs in them are the aqueous alteration products related to the alteration temperature [8]. Our study shows that Ryugu experienced as low temperature as CM chondrites during the parent body aqueous alteration, which is consistent with the discussion by [5].

**Conclusion:** In this study, organic sulfur functional groups were identified from the IOM isolated from Ryugu samples by S-XANES. Our results indicate that reductive organic sulfur components, i.e., organic sulfides (C-S-S-C, C-S-C), are dominant relative to oxidized organic sulfurs in Ryugu IOM. Ryugu IOM experienced low-temperature parent body aqueous alteration.

## References

[1] Tachibana S. et al. 2014. *Geochemical Journal* 48:571–587. [2] Yada T. et al. 2022. *Nature Astronomy* 6:214–220. [3] Yabuta, H. et al. 2022, *Science*, under review. [4] Yokoyama T. et al. 2022. *Science*, eabn7850. [5] Nakamura T. et al. 2022.

Science, abn8671. [6] Ito M. et al. 2022. *Nature Astronomy*, <https://doi.org/10.1038/s41550-022-01745-5>. [7] Schmitt-Kopplin Ph. et al. 2010. *PNAS* 107:2763–2768. [8] Orthous-Daunay FR. et al. 2010. *Earth and Planetary Science Letters* 300:321–328. [9] Bose M. et al. 2017. *Meteoritics & Planetary Science* 52:546–559. [10] Suga H. et al. 2021. *Minerals* 11:514.

**The Hayabusa2-initial-analysis Organic Macromolecule and Core Teams:** H. Yabuta, G. D. Cody, C. Engrand, Y. Kebukawa, B. De Gregorio, L. Bonal, L. Remusat, R. Stroud, E. Quirico, L. R. Nittler, M. Hashiguchi, M. Komatsu, E. Dartois, J. Mathurin, J. Duprat, T. Okumura, Y. Takahashi, Y. Takeichi, D. Kilcoyne, S. Yamashita, A. Dazzi, A. Deniset-Besseau, S. Sandford, Z. Martins, Y. Tamenori, T. Ohigashi, H. Suga, D. Wakabayashi, M. Verdier-Paoletti, S. Mostefaoui, G. Montagnac, J. Barosch, K. Kamide, M. Shigenaka, L. Bejach, T. Noguchi, H. Yurimoto, T. Nakamura, R. Okazaki, H. Naraoka, K. Sakamoto, S. Tachibana, S. Watanabe, and Y. Tsuda

# Investigating the noble gas and nitrogen relationship between Ryugu and other carbonaceous chondrites

M. W. Broadley<sup>1</sup>, D. J. Byrne<sup>1</sup>, E. Füre<sup>1</sup>, L. Zimmerman<sup>1</sup>, B. Marty<sup>1</sup>, R. Okazaki<sup>2</sup>, T. Yada<sup>3</sup>, F. Kitajima<sup>2</sup>, S. Tachibana<sup>3,4</sup>, K. Yogata<sup>3</sup>, K. Sakamoto<sup>3</sup>, H. Yurimoto<sup>5</sup>, T. Nakamura<sup>6</sup>, T. Noguchi<sup>7</sup>, H. Naraoka<sup>2</sup>, H. Yabuta<sup>8</sup>, S. Watanabe<sup>9</sup>, Y. Tsuda<sup>3</sup>, and the Hayabusa2 Initial Analysis Volatile Team

<sup>1</sup>Université de Lorraine, CNRS, CRPG, F-54000 Nancy France, <sup>2</sup>Kyushu University, Japan, <sup>3</sup>Institute of Space and Astronautical Science, JAXA, Japan, <sup>4</sup>University of Tokyo, Japan, <sup>5</sup>Hokkaido University, Japan, <sup>6</sup>Tohoku University, Japan, <sup>7</sup>Kyoto University, Japan, <sup>8</sup>Hiroshima University, Japan, <sup>9</sup>Nagoya University, Japan.

The Hayabusa2 mission of the Japan Aerospace Exploration Agency (JAXA) successfully returned surface material from the C-type asteroid (162173) Ryugu to Earth. This material has now been classified as closely resembling CI-type chondrites, which are the most chemically pristine meteorites. The analysis of material from the surface of Ryugu therefore provides a unique opportunity to analyze the volatile composition of material that originated from a CI-type asteroid [1] without complications arising from terrestrial contamination. Given their highly volatile nature, the noble gas and nitrogen inventories of chondrites are highly sensitive to different alteration processes on the asteroid parent body, and to terrestrial contamination.

We investigated at CRPG Nancy (France) the nitrogen and noble gas signature of two grains collected from the first and second touchdown sites [2] to provide an insight into the formation and alteration history of Ryugu. We find that the concentration of trapped noble gas in the Ryugu grains is greater than the average composition of previously measured CI chondrites. The trapped noble gases are primarily derived from phase Q, although a significant contribution of presolar nanodiamonds Xe-HL is noted. The large noble gas concentrations coupled with a significant contribution of presolar nanodiamonds suggests that the Ryugu grains may represent some of the most primitive unprocessed material from the early solar system.

In contrast to the noble gases, the abundance of nitrogen and  $\delta^{15}\text{N}$  composition of the two Ryugu grains are lower than the average CI chondrite value. We attribute the lower nitrogen abundances and  $\delta^{15}\text{N}$  measured in this study to the preferential loss of a  $^{15}\text{N}$ -rich phase from our grains during aqueous on a parent planetesimal. The analyses of other grains returned from Ryugu have shown large variations in nitrogen concentrations and  $\delta^{15}\text{N}$  indicating that alteration fluids heterogeneously interacted with material now present on the surface of Ryugu. Finally, the ratio of trapped noble gases to nitrogen is higher than CI chondrites, and is closer to refractory phase Q and nanodiamonds. This may indicate that Ryugu experienced aqueous alteration that led to the significant loss of nitrogen likely from soluble organic matter hosted in our two grains without significant modification of the noble gas budget, which is primarily hosted in insoluble organic matter and presolar diamonds and is more resistant to aqueous alteration.

## References

[1] Yokohama et al. 2022 Science DOI: [10.1126/science.abn7850](https://doi.org/10.1126/science.abn7850). [2] Okazaki et al. Science, Accepted.

# Nitrogen isotopes in Ryugu return samples revealed by the stepwise combustion analysis, in comparison with CI falls and Antarctic finds

Ko Hashizume<sup>1</sup>, Akizumi Ishida<sup>2</sup>, Ayano Chiba<sup>1</sup>, Ryuji Okazaki<sup>3</sup>, Toru Yada<sup>4</sup>, Fumio Kitajima<sup>3</sup>, Hisayoshi Yurimoto<sup>5</sup>, Tomoki Nakamura<sup>2</sup>, Hiroshi Naraoka<sup>3</sup>, Takaaki Noguchi<sup>6</sup>, Hikaru Yabuta<sup>7</sup>, Shogo Tachibana<sup>8</sup>, Sei-ichiro Watanabe<sup>9</sup>, Kanako Sakamoto<sup>4</sup> and Yuichi Tsuda<sup>4</sup>

<sup>1</sup>Faculty of Science, Ibaraki University, <sup>2</sup>Department of Earth Science, Tohoku University, <sup>3</sup>Department of Earth and Planetary Sciences, Kyushu University, <sup>4</sup>Institute of Space and Astronautical Science, Japan Aerospace Exploration Agency, <sup>5</sup>Department of Earth and Planetary Sciences, Hokkaido University, <sup>6</sup>Division of Earth and Planetary Sciences, Kyoto University, <sup>7</sup>Department of Earth and Planetary Systems Science, Hiroshima University, <sup>8</sup>UTokyo Organization for Planetary and Space Science, The University of Tokyo, <sup>9</sup>Department of Earth and Environmental Sciences, Nagoya University

Nitrogen isotope ratio is a powerful tool in cosmochemistry to decipher the origin and evolution of planetary materials. The nitrogen isotope ratio  $^{15}\text{N}/^{14}\text{N}$ , usually expressed by the delta notation,  $\delta^{15}\text{N} \equiv [(^{15}\text{N}/^{14}\text{N})/(^{15}\text{N}/^{14}\text{N})_{\text{AIR}} - 1] \times 1000$  (‰), exhibits large variations among different meteorites (Fig. 1). The isotope ratio of nitrogen, being a typical volatile element, is particularly useful to constrain the formation and evolution processes of planetary atmosphere for Earth and other rocky planets. Viable Earth formation models assume that CI/CM-like volatile-rich carbonaceous chondrites may have contributed as one of the important volatile sources for Earth, if not entirely on the source for the rocky body of this planet. CI chondrites, the most volatile-rich chondritic group known so far, exhibit  $\delta^{15}\text{N}$  values typically around +40 ‰. The higher  $\delta^{15}\text{N}$  values for the CI chondrites than for the present Earth atmosphere may impose important constraints on the formation and evolution history of the Earth atmosphere.

The texture and mineralogical composition of Ryugu samples are similar to CI chondrites. Three fall meteorites categorized as CI chondrites, Alais, Ivuna and Orgueil, have been studied so far for nitrogen isotopes. However, recent search on the vast stock of Antarctic meteorites has revealed that there exist several Antarctic meteorites which exhibit similar texture and mineralogical composition with the fall CI chondrites. Though similar, these potential CI Antarctic meteorites still exhibit marked difference from the CI falls, particularly from the volatile-element points of view: The majority of phyllosilicates are dehydrated in these Antarctic CI meteorites, while the phyllosilicates of CI falls mostly remain hydrated [4]. Fig. 2 compares bulk nitrogen isotope composition of Ryugu samples with those of CI chondrites, falls (Alais, Ivuna and Orgueil) and an Antarctic find (Y-980115). Interestingly, the  $\delta^{15}\text{N}$  values are correlated with the nitrogen concentrations: lower the concentration, lower the  $\delta^{15}\text{N}$  value. Note that this correlation is not compatible with the one we normally expect to occur by Rayleigh-distillation type devolatilization process, nor by addition of a terrestrial contamination at different degrees. Apparently, an unknown isotope fractionation (or mixing) effect in the nitrogen isotope composition has emerged among the CI-chondrite family.

The stepwise analyses may provide isotope “fingerprints” to compare the identities of planetary materials. By this method, we may distinguish possible endmembers co-existing in the samples. Fig. 3 demonstrates the usefulness of this method, for example, by the profiles obtained from a Ryugu bulk sample, compared with the one for CI chondrite Orgueil. These profiles provide information, not only the bulk  $\delta^{15}\text{N}$  value and bulk N and C concentrations, but include points such as, (a) presence of a nitrogen component easily combustible at low (>200°C) temperatures with  $\delta^{15}\text{N} < +10$  ‰, (b) a component released

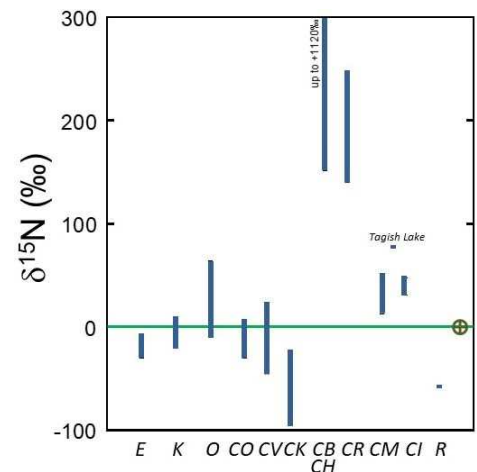


**Fig 1.** Bulk nitrogen isotope composition among different meteorites. Compilation by Hashizume (2015) [1]. Important isotope data beyond this range include protosolar composition (-380 ‰; Marty et al, 2011 [2]) or cometary range (+600 - +1000‰; Marty et al, 2016 [3])

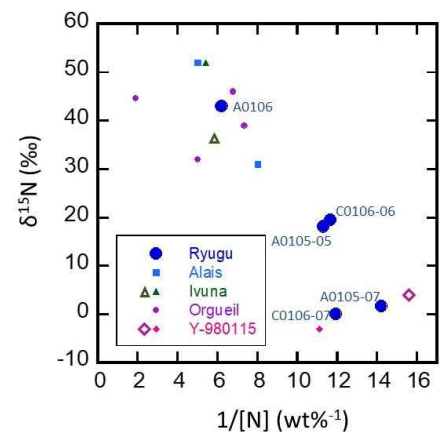


**Fig 2.** Bulk nitrogen isotope composition of Ryugu samples and CI chondrites. Ryugu data labelled A0105-07 and C0106-07 are reported in [5] (Ibaraki data); A0105-05 and C0106-06 in [6] (Nancy data); A0106 in [7] (JAMSTEC data). The other solid marks are literature bulk data for CI chondrites from [8-13]. Open marks (Ivuna and Y-980115) are sums of unpublished stepwise combustion data recently acquired at Ibaraki Univ.

spike-wise at  $\sim 500^{\circ}\text{C}$  with  $\delta^{15}\text{N} \ll 0$  ‰, which is inferred to be hosted by presolar nano-diamonds, (c) one released at  $600\text{--}800^{\circ}\text{C}$  exhibits a plateau  $\delta^{15}\text{N}$  value of  $+17$ ‰, and (d) finally the one released at  $1100^{\circ}\text{C}$  and above with a  $\delta^{15}\text{N}$  value as low as  $-20$ ‰. Apparently, nitrogen in Ryugu consist of several components with distinct origins. The combustion profile of Orgueil, though shows partially similar isotope signature with Ryugu, for example the one presumably from presolar microdiamonds, exhibits generally  $\delta^{15}\text{N}$  higher than Ryugu by several tens of ‰, and higher N concentrations. The differences are particularly prominent at low temperature range below  $600^{\circ}\text{C}$ , which is generally considered to be the range where N from the organic matter is released. Seemingly the organic matter with  $\delta^{15}\text{N}$  values as high as  $+60$ ‰ is missing in Ryugu, which could correspond to the “missing component” inferred by comparing the bulk composition for samples belonging to the CI chondrite family (Fig. 2). It is worth to note that, though the missing component could be inferred to be an organic component from the combustion temperature, it seems to be decoupled with the bulk of carbon, and could be a component with a peculiar chemical composition with much higher N/C ratios than the bulk composition.

In this presentation, we will compare the stepwise combustion profiles obtained for Ryugu, with those of Ivuna and Y-980115 recently obtained using the same facility equipped at Ibaraki University. Though part of the Ryugu data (A0105-07 and C0106-07) exhibit similar bulk nitrogen concentrations and  $\delta^{15}\text{N}$  values with Y-980115, we will demonstrate that the combustion profiles appear quite different, possibly suggesting that the N isotope evolution mechanism could be different between these two kinds of CI-like samples.

## References

- [1] Hashizume K. 2015. In “Encyclopedia of Astrobiology” doi:10.1007/978-3-642-27833-4\_1065-3. [2] Marty B. et al. *Science* 332:1533. [3] Marty B. et al. 2016. *Earth and Planetary Science Letters* 441:91. [4] King AJ. et al. 2019. *Geochemistry* 79:125531. [5] Okazaki R. et al. 2022. Abstract #1348. 53rd LPSC. [6] Byrne DJ. et al. 2022. Abstract #2096. 53rd LPSC. [7] Naraoka H. et al. 2022. Abstract #1781. 53rd LPSC. [8] Kerridge JF. 1985. *Geochimica et Cosmochimica Acta* 49:1707. [9] Robert F. & Epstein S. 1982. *Geochimica et Cosmochimica Acta* 46:81. [10] Yang J. & Epstein S. 1983. *Geochimica et Cosmochimica Acta* 47:2199. [11] Grady MM. et al. 2002. *Meteoritics & Planetary Science* 37:713. [12] Pearson VK. et al. 2006. *Meteoritics & Planetary Science* 41:1899. [13] Chan QHS. et al. 2016. *Earth, Planets and Space* 68:7.

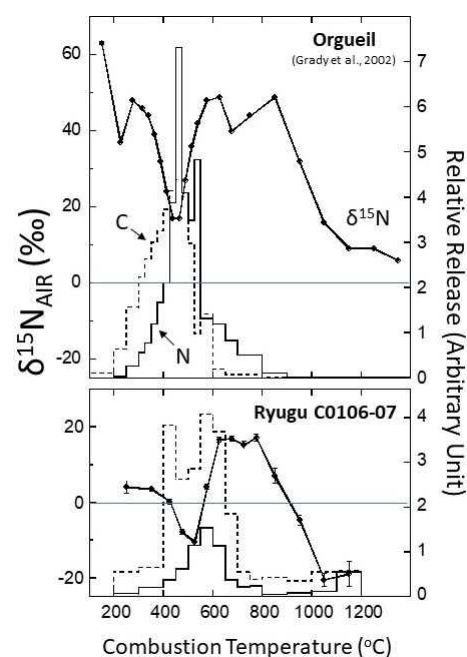


**Fig 3.** Comparison of stepwise combustion profiles for Ryugu sample C0106-07 (btm) obtained at Ibaraki Univ, and literature data [11] for Orgueil (top). The concentrations are plotted in arbitrary unit, although the areas of the bars between different temperature ranges, and also between the two samples for the same element correctly represent the relative concentrations.

# Visible to Near-Infrared Spectrophotometry of C0002 Powder Samples of Asteroid 162173 Ryugu in Comparison with ONC-T and NIRS3 Instruments Onboard Hayabusa2 Spacecraft

T. Hiroi<sup>1</sup>, R. E. Milliken<sup>1</sup>, K. M. Robertson<sup>1</sup>, C. D. Schultz<sup>1</sup>, K. Amano<sup>2</sup>, T. Nakamura<sup>2</sup>, H. Yurimoto<sup>3</sup>, T. Noguchi<sup>4</sup>, R. Okazaki<sup>5</sup>, H. Yabuta<sup>6</sup>, H. Naraoka<sup>5</sup>, K. Sakamoto<sup>7</sup>, S. Tachibana<sup>8</sup>, T. Yada<sup>7</sup>, M. Nishimura<sup>7</sup>, A. Nakato<sup>7</sup>, A. Miyazaki<sup>7</sup>, K. Yogata<sup>7</sup>, M. Abe<sup>7</sup>, T. Okada<sup>7</sup>, T. Usui<sup>7</sup>, M. Yoshikawa<sup>7</sup>, T. Saiki<sup>7</sup>, S. Tanaka<sup>7</sup>, T. Fuyuto<sup>9</sup>, S. Nakazawa<sup>7</sup>, S. Watanabe<sup>10</sup>, Y. Tsuda<sup>7</sup>, S. Sasaki<sup>11</sup>, H. Kaiden<sup>12</sup>, K. Kitazato<sup>13</sup>, M. Matsuoka<sup>14</sup>, and E. Tatsumi<sup>15</sup>

<sup>1</sup>Brown University, <sup>2</sup>Tohoku University, <sup>3</sup>Hokkaido University, <sup>4</sup>Kyoto University, <sup>5</sup>Kyusyu University, Japan, <sup>6</sup>Hiroshima University, <sup>7</sup>JAXA Institute of Space and Astronautical Science, <sup>8</sup>University of Tokyo, <sup>9</sup>Kanagawa Institute of Technology, <sup>10</sup>Nagoya University, <sup>11</sup>Osaka University, <sup>12</sup>National Institute of Polar Research, <sup>13</sup>University of Aizu, <sup>14</sup>National Institute of Advanced Industrial Science and Technology, <sup>15</sup>Instituto de Astrofisica de Canarias.

## Samples and Spectrophotometric Measurements

Powder samples of the largest sampled stone C0002 of asteroid 162173 Ryugu returned by Hayabusa2 mission were loaned for visible and near-infrared (VNIR) spectrophotometric studies. The powder samples were produced by physical-strength measurements and were partially contaminated with a glue (glycol phthalate). Part of the powder was washed with acetone, which turned it into a fine powder (<125 μm estimate). Large glue fragments were handpicked from the remaining coarse powder (125-500 μm estimate) and a bulk powder sample was produced by combining the two powder samples.

Bidirectional VNIR reflectance spectra (0.3-2.6 μm) of the samples were measured at NASA Reflectance Experiment Laboratory (RELAB) using its bidirectional reflectance spectrometer at the standard viewing geometry of 30° incidence and 0° emergence angles, and their photometric properties were measured at a limited number of viewing geometries. The photometric property of a Labsphere Spectralon standard was measured relative to the standard viewing geometry at 550 nm in wavelength.

Biconical Fourier-transform infrared (FTIR) reflectance spectra (1-100 μm) of the samples were measured in a dry-air purged environment. The VNIR and FTIR spectra were combined at 2.5 μm in wavelength by scaling the FTIR reflectance to the VNIR reflectance.

## Spectrophotometric Analyses

Phase-angle dependency of the powder samples at 550 nm in wavelength is plotted in Fig. 1, and VNIR-FTIR spectra up to 4 μm are plotted in Fig. 2 along with sample photos under a microscope. The phase curve in Fig. 1 shows much brighter albedo and lower inclination than those obtained by ONC-T measurements in proximity of asteroid Ryugu [1]. It may be due to the difference between the flatter surface of the powder sample compared with the rough asteroid surface that includes shadows. Further photometric modeling analysis is warranted.

The OH and H<sub>2</sub>O absorption bands near 3 μm in spectra shown in Fig. 2 were analyzed in the same manner as [2]. Natural log reflectance spectra of the powder samples were fit with a linear-in-wavelength continuum background and Gaussians (in wavenumber) over the wavelength range of ~2.6-3.6 μm (variable depending on spectral shape). One of the results (fine powder) is shown in Fig. 3. Because the first two Gaussian bands (labeled as 1 and 2 in Fig. 3) are believed to be characteristic of carbonaceous chondrite classes [2], their

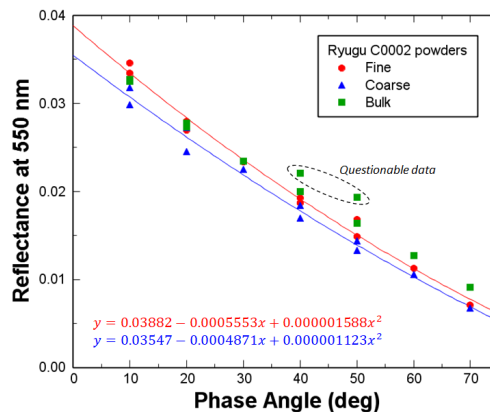


Fig. 1. Phase-angle dependency of reflectances of C0002 powder samples at 550 nm in wavelength.

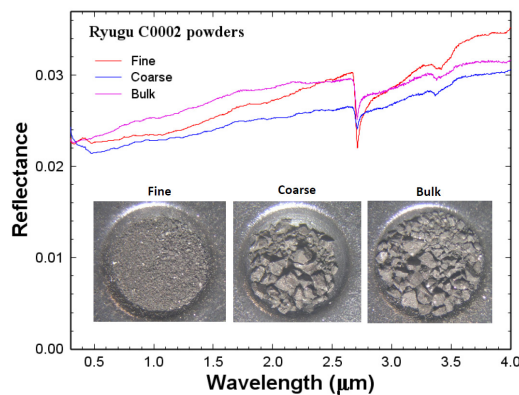


Fig. 2. VNIR-FTIR spectra (0.3-4 μm) and photos of C0002 powder samples. Cup diameter is 4 mm.

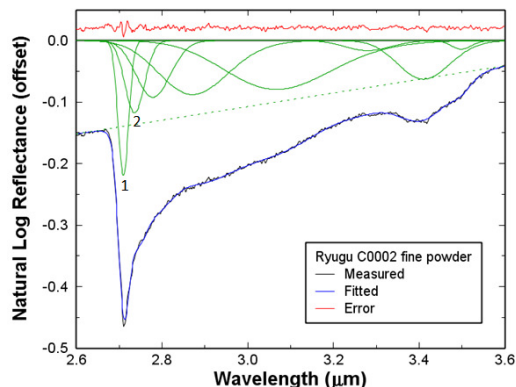


Fig. 3. Gaussian fitting of C0002 fine powder spectrum.

Band 1 centers and Band 1 / Band 2 strength ratios are plotted in Fig. 4. Ryugu C0002 powders all plot very close to unheated CI1 chondrites and Ivuna heated up to 400°C. This result is consistent with previous studies of Ryugu being mostly unheated CI1 chondrite [e.g., 3], and low-degree heating may not be detected by this method.

### Comparison with ONC-T and NIRS3 Observations

Shown in Fig. 5 is a plot of linear combinations of the VNIR-FTIR spectra of the C0002 fine and coarse powder samples to match average spectra of representative (but different) areas of Ryugu acquired by ONC-T and NIRS3. Most of the ONC-T band reflectance values, overall spectral shape, and 2.7 μm absorption band strength could be matched.

However, when the 2.7 μm band region is closely examined, there are significant mismatches between the NIRS3 and C0002 spectra. The NIRS3 spectrum shows absorption bands at 2.65 and 2.81 μm which are absent in C0002 spectrum. If this is not due to NIRS3 data calibration errors, there may be some unstable phases lost during the sample recovery.

Another mismatch is the 2.7 μm band center position. Fig. 6 shows the NIRS3 spectrum and the modeled C0002 spectrum with its wavelength resolution matched with that of NIRS3 spectrum (18 nm). While the NIRS3 spectrum (open black squares) shows the band center at around 2.72 μm asymmetrically expanded toward the longer wavelength, the modeled C0002 powder spectrum (solid purple circles) shows the band center clearly at a shorter wavelength near 2.71 μm. When the C0002 powder spectra are artificially shifted toward the longer wavelength by 6 nm before resampling for the NIRS3 resolution, the resulting modeled spectrum (open purple circles) matches with the NIRS3 spectrum much better. A difference in band position is consistent with spectra of ejecta from an artificial crater showing shorter 2.7 μm band positions [4].

### Summary and Discussion

If the C0002 powder samples represent the average surface material of asteroid Ryugu, this study indicates that the global space weathering may have occurred mainly by solar wind that caused the 2.7 μm absorption band center to be shifted toward a longer wavelength [e.g., 5]. If such space weathering occurred, the 2.7 μm band strength and the visible spectra measured with ONC-T might have been altered as well. This would influence the physical interpretation of the model fits shown in Fig. 5.

### References

- [1] Tatsumi E. et al. 2020. A&A 639:A83. [2] Hiroi T. et al. 2021. Polar Science 29:100723. [3] Yokoyama T. et al. 2022. Science 10.1126:7850. [4] Kitazato K. et al. 2021. Nature Astronomy 5:246. [5] Lantz C. et al. 2015. A&A 577:A41.

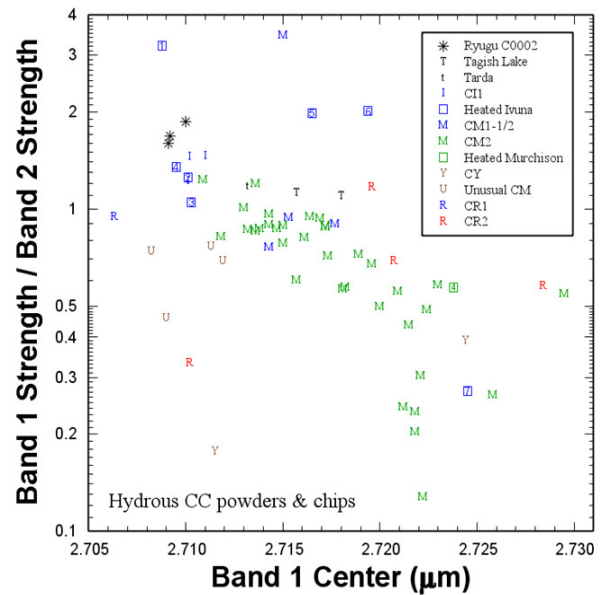


Fig. 4. Band 1 center vs. Band 1 / Band 2 strength ratio of C0002 powder samples plotted with hydrous carbonaceous chondrites (modified from [2]).

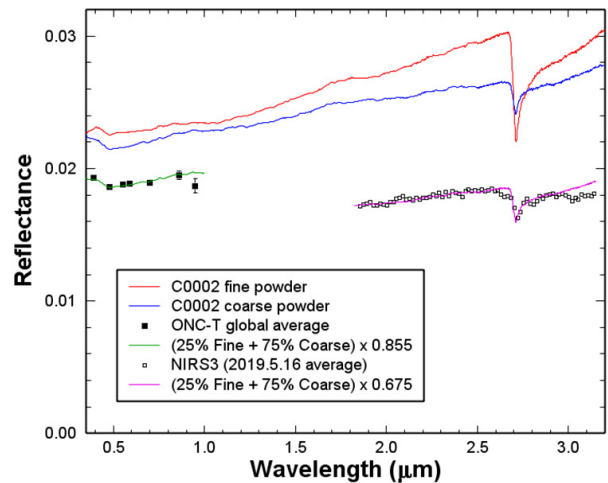


Fig. 5. Comparison of C0002 powder spectra with ONC-T and NIRS3 data.

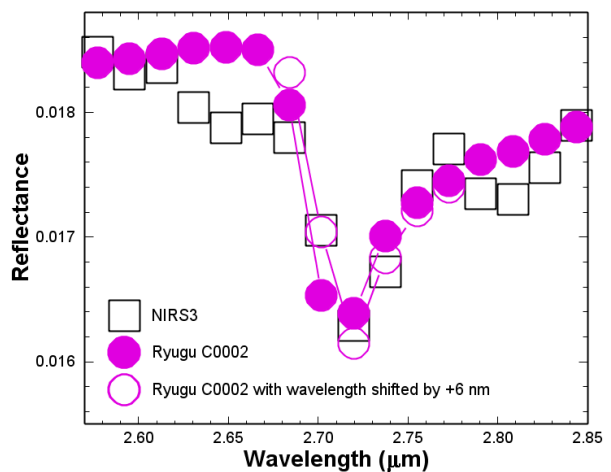


Fig. 6. Matching of the 2.7 μm absorption band feature between the modeled C0002 powder spectra and NIRS3 spectrum in Fig. 5.

# Reflectance spectrum of Ryugu grains and their acid-extracted residues in the UV–VIS range

K. Yumoto<sup>1</sup>, H. Yabuta<sup>2</sup>, S. Sugita<sup>1</sup>,

The Hayabusa2 initial analysis IOM team, and the Hayabusa2 Initial Analysis Core team

<sup>1</sup>*Univ. of Tokyo, Japan.*

<sup>2</sup>*Hiroshima Univ., Japan.*

**Introduction:** Reflectance spectrum in the ultraviolet to visible (UV–VIS) range is among the most frequently used wavelength range for observations of main-belt C-complex asteroids. Furthermore, distinctive spectral differences (e.g., spectral slope, absorption at UV) have been reported among C-complex asteroids [1]. However, their interpretation is not necessarily straightforward. This is because the UV–VIS spectrum is controlled by various physical (e.g., grain size) and/or chemical (e.g., mineralogy) state of the reflector. Thus, it is difficult to translate the UV–VIS spectral properties into physically and mineralogically well-defined constraint(s) on asteroid materials.

Studies on the UV–VIS spectra of samples returned from asteroid Ryugu may help us resolve this problem. This is because the physical/chemical state of the returned samples have been studied in detail and pre-processing of the samples allows us to control the sample state (e.g., extraction of certain minerals by acid treatments). Remote sensing by the Optical Navigation Camera (ONC) onboard Hayabusa2 revealed a dark/flat and homogeneous UV–VIS spectrum on the surface of Ryugu [2]. The dark/flat nature of the spectrum was confirmed by initial description of the returned samples [3, 4]. However, grain-to-grain spectral variation was substantially higher than those observed by remote sensing [5]. The variation in reflectance has been attributed to specular reflections caused by micro-scale facets, which were not resolved by remote sensing [5]. Such a result suggests that the texture of grains and abundance of opaque minerals with high reflectivity in the UV–VIS range can highly affect the reflectance of C-complex asteroids. However, the specific (sets of) minerals and/or organic matter that affect the spectra of returned samples have not been identified yet.

In this study, we compared the UV–VIS spectra of intact Ryugu grains with those of acid-extracted residues to evaluate how insoluble organic matter (IOM) contribute to Ryugu’s dark and flat spectrum.

**Samples and methods:** We measured the UV–VIS spectra of returned samples with and without acid treatments that dissolve specific minerals: intact (i.e., un-extracted) grains, HCl-extracted residues, and HCl/HF-extracted residues. All samples were allocated to and processed by the Hayabusa2 IOM team. We measured 50 intact grains from aggregate samples A0106, A0108, and C0109 and 35 grains in the HCl-extracted residues from A0108. Minerals, such as carbonates, sulfides, and magnetite are removed by HCl extraction, and the residue mainly comprises of phyllosilicates and IOM. We also measured 19 grains in the HCl/HF-extracted residues from C0002 and C0107. HCl/HF extraction only leaves IOM within the residue. The sizes of all grains ranged from ~10  $\mu\text{m}$  to 200  $\mu\text{m}$  except for one ~1 mm intact grain from A0108.

The UV–VIS spectra were measured by a high-resolution multi-band spectrometer developed at the University of Tokyo. The spatial resolution is ~2  $\mu\text{m}$  at 550 nm with a 300  $\mu\text{m}$   $\times$  300  $\mu\text{m}$  field of view. The spectrometer is equipped with 25 narrow (10 nm width) band-pass filters from 230 to 1000 nm. Energy of the light power was reduced (30  $\mu\text{W}$  at 550 nm) to avoid sample alteration. A standard diffuse reflector with 99% reflectance (Spectralon/Labsphere) was used for radiometric calibration.

**Results and Discussion:** The reflectance image of the largest grain measured in this study is shown in Fig. 1. Areas with high reflectance in Fig. 1 are specular reflections. Such specular reflections were also observed in acid-extracted residues. These photometric effects were not corrected in our analysis but reflectance from the entire grain (within the dashed curve in Fig. 1) were integrated to obtain the average reflectance for each grain. The spectrum of a typical grain for each of the three mineralogic composition type is shown in Fig. 2. These spectra show that mineralogy have a significant effect on the 1) reflectance, 2) UV absorption feature, and 3) VIS spectral slope as follows.

1. *Reflectance:* Though reflectance has large grain-to-grain variation, Fig. 2 shows that phyllosilicate + IOM residues (i.e., HCl-extracted residues) have a significantly darker reflectance. Such correlation of reflectance with mineralogy provides insights into the reason for the dark nature of carbonaceous materials. Our result implies that the mixing state of phyllosilicates with IOMs may be important in effectively darkening the carbonaceous material. However,

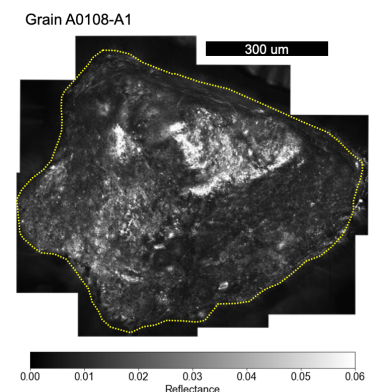


**Fig 1** Reflectance image of the largest grain (from A0108) measured in this study. The dashed curve shows the rim of the grain.

reflectance of acid-extracted residues can be affected by physical and/or chemical alteration caused by the extraction process. Characterization of such alteration is needed to verify the implication of our result.

2. *UV absorption feature*: Fig. 2 shows that though spectra of intact grains are flat throughout the UV–VIS range, spectra of acid-extracted residues show a broad UV absorption centered at ~300 nm. The absorption shape of IOM in Ryugu samples, which is characterized by steepening of the spectral slope from VIS to UV, is consistent with those in Murchison meteorites [6]. Meteoritic studies show that such UV absorption may be caused by abundance of C-H bonds in organics [7] or deficit of magnetite [8]. Since acid extraction removes magnetite and increases the concentration of IOM in the residues, our result is consistent with both hypotheses.
3. *VIS slope*: Fig. 2 shows that IOMs exhibit a redder slope in the VIS range. Such trend is consistent with measurements of IOMs in carbonaceous meteorites [6, 9].

These correlation of the spectra with demineralization can be clearly observed in Fig. 3; residues have deeper UV absorption and IOMs have redder VIS slope. This result suggests that variations in UV absorption and spectral slope observed among C-complex asteroids [1] may represent difference in relative abundance of organics to other acid-soluble minerals.

**Conclusion:** We measured the UV–VIS spectra of Ryugu returned samples and their acid-extracted residues to evaluate how IOM contributes to the dark and flat spectra of Ryugu. Our results show that a variation of constituting minerals/organics, especially demineralization of opaque minerals with higher reflectivity and increase in concentration of IOM, has a significant effect on the reflectance, UV absorption feature, and VIS slope of Ryugu returned samples. This result implies that spectral variation in the UV–VIS range observed among C-complex asteroids may represent chemical variation such as abundance of organics and other acid-soluble minerals.

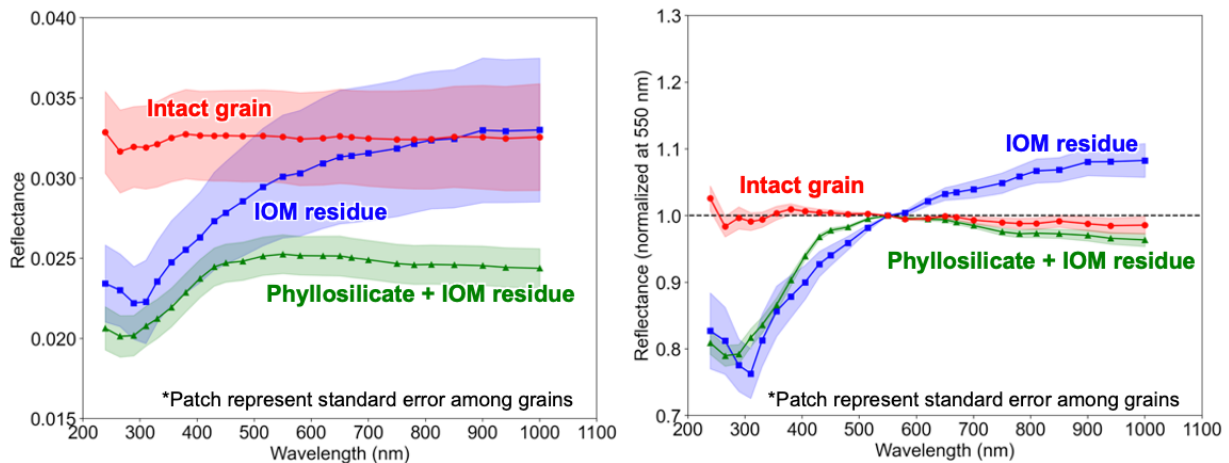


Fig 2 (Left) Average reflectance spectrum for each of the mineralogic composition. (Right) Reflectance spectrum after normalization at 550 nm. The patch represents the standard error observed among grains.

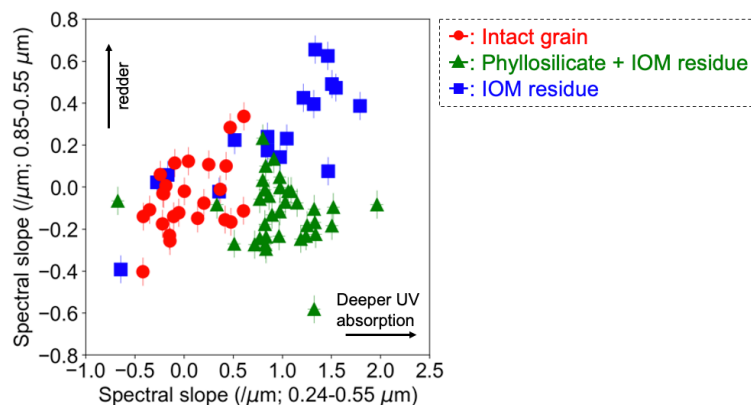


Fig 3 Correlation plot between UV and VIS spectral slope. Each plot shows the spectrum for each grain measured in this study.

**References:** [1] Bus & Binzel (2002). *Icarus*, 158(1), 146-177. [2] Sugita et al. (2019). *Science*, 364(6437), eaaw0422. [3] Yada et al. (2021) *Nat. Astron.*, 6(2), 214-220. [4] Cho et al. (2022). *PSS*, 221, 105549. [5] Yumoto et al. (2022). JpGU, #C002365. [6] RELAB, PDS Geosciences Node Spectral Library. [7] Hendrix et al. (2016) *MAPS*, 51(1), 105-115. [8] Hendrix et al. (2019). *GRL*, 46(24), 14307-14317. [9] Kaplan et al. (2019). *MAPS*, 54(5), 1051-1068.

# Nano-infrared spectroscopy of Ryugu samples using AFM-IR measurement

Van T. H. Phan<sup>1</sup>, Pierre Beck<sup>1</sup>, Rolando Rebois<sup>1</sup> and Takaaki Noguchi<sup>2</sup>, the Hayabusa2-initial-analysis Sand team.

<sup>1</sup>Université Grenoble Alpes, CNRS, Institut de Planétologie et d'Astrophysique de Grenoble (IPAG), France

<sup>2</sup>Kyoto University, Division of Earth and Planetary Science, Kyoto, Japan

**Introduction:** In late 2020, samples of Ryugu (C-type) were collected from its asteroid and returned to Earth, led by the Japan Aerospace Exploration Agency (JAXA), thought to be similar in composition to CI chondrites<sup>1</sup>. Understanding how and under what conditions the organic matter interacted with inorganic phases, is a key step in hypothesizing the mechanism of accreted organic matter. This “fresh” carbonaceous material allows us to investigate the best preservation sample without terrestrial impact<sup>2</sup>. In addition, the “bulk” Ryugu samples also show some spectral reflectance bands corresponding to the NH-rich compounds<sup>3</sup>. Altogether, our study aims to characterize the mineralogy, organic matter and the possible N-bearing molecule. To gain insight into fine meteorites matrices containing an interplay of ingredients at the sub-micro scale, it requires analytical techniques with the sub micrometer spatial resolution to separate their composition and understand their petrographic relations. Infrared spectroscopy (IR) is an effective method and a non-destructive technique for molecular-atomic scale vibrations of organic and inorganic compounds in the extra-terrestrial materials<sup>4,5</sup>. However, conventional IR spectrometers use mirror-based optics to focus the beam on the sample and thus the spatial resolution is limited by the diffraction limit. This IR diffraction limitation can be overcome by using AFM-IR (Atomic Force Microscopy-Infrared Spectroscopy), based on the combination of infrared spectroscopy and atomic force microscopy to efficiently distinguish spectral signatures of the different constituents<sup>6,7</sup>.

Our study aims to characterize two different grains of Ryugu that can be affected by the weathering space prepared by “Min-pet fine team” (Sand team)<sup>8</sup> as crushed sample between two diamond windows, as well as two different Orgueil samples: one comes from the Paris Museum (Orgueil Museum) and the another one expected “fresher” kept in the sealed flask (Orgueil Flask) from collection of M. Bizzaro. Here, we report the comparison of AFM-IR results between Ryugu and Orgueil as a CI chondrite both in mineralogy and organic structure.

**Samples preparation and methods:** Two grains of Ryugu (P0032 and P0038), received from the Sand initial analysis team, were prepared by crushing 10 – 20  $\mu\text{m}$  fragments between two diamond windows. As with Ryugu, the Orgueil Museum and Orgueil Flask samples were also pressed down to the appropriate thickness for AFM-IR measurement. Before AFM-IR analysis, all samples were performed the micro-FTIR analysis to select the region of interests (ROI).

**IR spectroscopy and AFM-IR measurement:** The micro-infrared spectra were first analyzed with a Bruker Hyperion 3000 infrared microscope. The nano-IR measurements were obtained with a Bruker nanoIR3s at IPAG (Grenoble, France), which includes an AFM probe capable of scanning the sample and generating topographic images at nm vertical resolution. The AFM-IR measurement can be performed in two acquisition modes: AFM and chemical imaging, and local, single point IR spectrum. First, the wavenumber is fixed and the tip moves along the surface to obtain the AFM topography and IR absorption at the given wavenumber. Second, the position of the tip is fixed and the IR laser is tuned to the possible spectral range (2000 – 700  $\text{cm}^{-1}$  with the APE laser at IPAG) which provides the local absorption spectrum at the point of interest<sup>6</sup>.

**Results and Discussion:** We are able to characterize two bulk grains of Ryugu with the region of interest  $5 \times 5 \mu\text{m}^2$  (grain P0032) in the in Figure 1 and the ROI of  $3 \times 3 \mu\text{m}^2$  (grain P0038) in Figure 2.

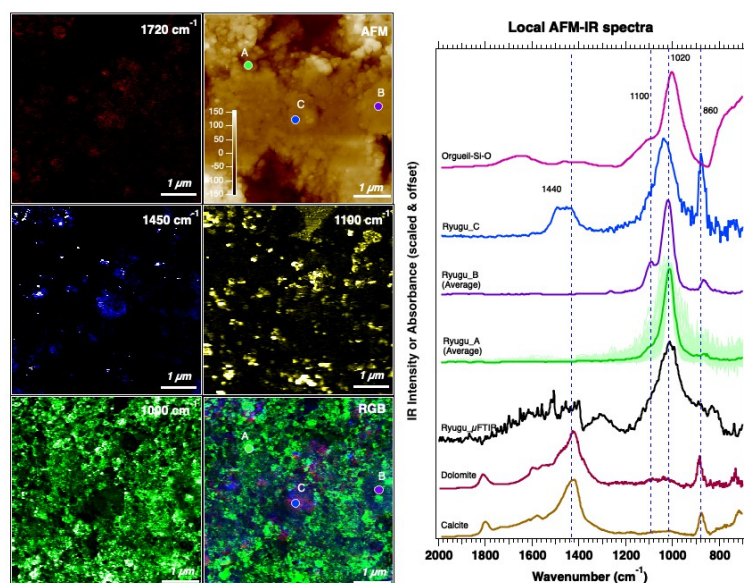


Figure 1. AFM-IR of a  $5 \times 5 \mu\text{m}^2$  region of interest (ROI) of grain P0032. Left images: AFM image, the AFM-IR images of 1720 (red), 1450 (blue), 1100 (yellow), 1000  $\text{cm}^{-1}$  (green) corresponding to C=O, carbonate, sulfate and Si-O; and RGB (red, green, blue) composition image from the combination of three AFM-IR absorption images: 1720, 1450 and 1000  $\text{cm}^{-1}$  respectively. Right panel: comparison of local AFM-IR spectra on the carbonate rich area (in blue), and the phyllosilicate area (in green) with phyllosilicate signature of Orgueil Flask,  $\mu$ -FTIR spectra of Ryugu, calcite and dolomite minerals.

In the first grain, P0032, AFM-IR images at different wavenumber were obtained at 1720, 1450, 1100 and 1000  $\text{cm}^{-1}$  in the left panel corresponding to carbonyl (C=O), carbonate, sulfate and phyllosilicate (Si-O), respectively (Figure 1). The three maps of 1720, 1450 and 1000  $\text{cm}^{-1}$  wavenumber were overlaid in the RGB composite image, allowed us to identify the two different domain compositions in the mapped area: the green area can be distinguished by a strong absorption at 1000  $\text{cm}^{-1}$  attributed to the presence of phyllosilicate; the blue/purple area shows a strong absorption at 1450  $\text{cm}^{-1}$  related to carbonate. Numerous spectra were obtained across this ROI shown in the right panel and compared to AFM-IR spectra of Orgueil Flask, dolomite, calcite and  $\mu$ -FTIR of the same P0032 grain. Spectrum A, the average of hundreds of spectra in the green region shows signature at 1020  $\text{cm}^{-1}$  corresponding to phyllosilicate (e.g., saponite, serpentine). Compared to the Orgueil phyllosilicate spectra, Ryugu is lack of a sulfate signature at 1100  $\text{cm}^{-1}$ . However, we observed that some purple areas have stronger absorption at 1100  $\text{cm}^{-1}$  and AFM-IR spectra also confirm the two peaks at 1100 and 840  $\text{cm}^{-1}$  (B spectrum). This Ryugu sample was collected in the fine-grained fraction, affected by space weathering<sup>8</sup>, the phyllosilicate-rich region can be modified. C spectrum in the blue region suggests the presence of carbonate with two strong signatures at 1440 and 860  $\text{cm}^{-1}$ , all indicative of dolomite or calcite.

In the second Ryugu grain, P0038, we first collected the different images at 1720 (red), 1450 (blue) and 1000  $\text{cm}^{-1}$  (green) in ROI of  $20 \times 20 \mu\text{m}^2$  and overlaid them in the RGB composite image in the upper left panel. We found a  $\sim 1 \mu\text{m}$ -diameter globule with strong absorption at 1720  $\text{cm}^{-1}$  corresponding to C=O in the organic material (Figure 2). Therefore, the ROI of  $3 \times 3 \mu\text{m}^2$  was selected to obtain the different images at 1720, 1600, 1450 and 1000  $\text{cm}^{-1}$ . The RGB composite (combined between the images at 1720, 1450 and 1000  $\text{cm}^{-1}$ ) show an organic globule in red with strong absorption at 1720  $\text{cm}^{-1}$ . Later, the contact AFM-IR spectra also confirm the presence of organic matter with two distinct features at 1720 and 1610  $\text{cm}^{-1}$  corresponding to C=O and C=C, respectively. Although the AFM-IR images only show the strong organic appearance, the AFM-IR spectra of organic globule still mixes with the minerals. Compared to the organic matter obtained at Orgueil described in<sup>9</sup>, the Ryugu organic material is more aromatic. The more diffuse organic may present in this ROI but still finely mixed with phyllosilicate.

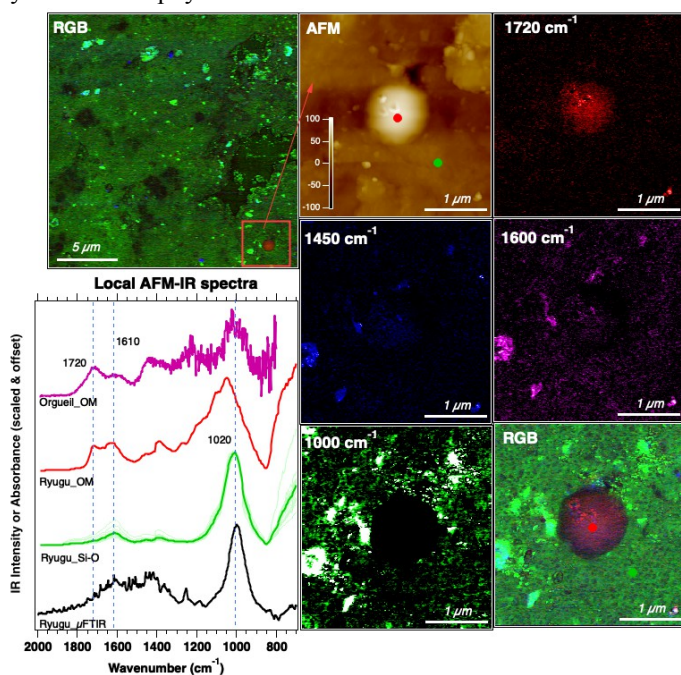


Figure 2. AFM-IR of a  $3 \times 3 \mu\text{m}^2$  region of interest (ROI) acquired with the NanoIR3s at IPAG (Grenoble, France) of grain P0038 from the RGB image of  $20 \times 20 \mu\text{m}^2$  region on the upper left panel. Right images: AFM image, the AFM-IR images of 1720 (red), 1600 (pink), 1450 (blue), 1000  $\text{cm}^{-1}$  (green) corresponding to C=O, C=C,  $\text{CO}_3/\text{CH}_2$  bend, and Si-O; and RGB (red, green, blue) composition image from the combination of three AFM-IR absorption images: 1720, 1450 and 1000  $\text{cm}^{-1}$ , respectively. Lower left panel: comparison of local AFM-IR spectra on the organic globule (red), and the phyllosilicate area (green) with organic matter of Orgueil and  $\mu$ -FTIR spectra of Ryugu.

**Conclusion:** The complete results and discussion of this study will be presented at the conference. So far, we confirm that the AFM-IR technique allows us to disentangle the IR signatures of phyllosilicate, carbonate and organic matter in Ryugu at the sub-micron scale. In mineralogy, compared to Orgueil, the sulfate signatures almost absent from the phyllosilicate, but some modifications in Si-O-rich areas were observed. In the organic structure, the weak organic signature is diffuse and significantly intermixed with phyllosilicate, similar to the diffuse organic of Orgueil. A  $1 \mu\text{m}$ -organic globule was also observed with clear C=O and C=C features in its structure. This organic matter globule is more aromatic compared to the organic matter in Orgueil meteorites.

**Reference:** [1] Yokoyama T. et al. 2022 *Science* (80). [2] Yada T. et al. 2021 *Nat Astron*. [3] Pilorget C. et al. 2022. *Nat Astron*. [4] Orthous-Daunay FR. et al. 2013. *Icarus*. [5] Phan VTH. et al. 2021. *Spectrochim Acta - Part A Mol Biomol Spectrosc*. [6] Dazzi A, Prater CB. 2017. *Chem Rev*. [7] Mathurin J. et al. 2019. *Astron Astrophys*. [8] Noguchi T. et al. 2022. Abstract #1747. 53rd LPSC. [9] Phan VTH. et al. 2022. *Meteorit Planet Sci*.

## Multi-scale variations of the ~2.7 $\mu\text{m}$ feature in Ryugu samples, observed by MicrOmega

<sup>1</sup>Le Pivert-Jolivet, T.; <sup>1,2</sup>Pilorget, C.; <sup>1</sup>Brunetto, R.; <sup>1</sup>Bibring, J.-P.; <sup>3</sup>Nakato, A.; <sup>1</sup>Hamm, V.; <sup>3,4</sup>Hatakeda, K.; <sup>1</sup>Lantz, C.; <sup>1</sup>Loizeau, D.; <sup>1,5</sup>Riu, L.; <sup>3</sup>Yogata, K.; <sup>1</sup>Baklouti, D.; <sup>1</sup>Poulet, F.; <sup>1</sup>Aléon-Toppani, A.; <sup>1</sup>Carter, J.; <sup>1</sup>Langevin, Y.; <sup>3,6</sup>Okada, T.; <sup>3</sup>Yada, T.; <sup>3,6</sup>Usui, T. and the MicrOmega ISAS Curation Team

<sup>1</sup>IAS, Université Paris-Saclay, CNRS, France, <sup>2</sup>Institut Universitaire de France, <sup>3</sup>Institute of Space and Astronautical Science, Japan Aerospace Exploration Agency, <sup>4</sup>Marine Works Japan, Ltd, <sup>5</sup>ESAC, ESA, Madrid, Spain, <sup>6</sup>University of Tokyo, Bunkyo, Tokyo 113-0033, Japan

Hayabusa2 is the first space mission to study and collect samples from a C-type asteroid. In December 2020, the spacecraft brought back to Earth ~5.4g of materials from the surface of asteroid (162173) Ryugu. The samples were collected from two different sites TD1 and TD2 [1] at the surface of the asteroid. The second touchdown was performed near the artificial crater created by the small carry-on impactor [2] to collect both surface and subsurface materials. The samples were delivered to JAXA (Japan Aerospace eXploration Agency) Extraterrestrial Curation Center for preliminary analyses. They were extracted from chambers A and C, corresponding to TD1 and TD2 respectively, weighed and analyzed in a controlled N<sub>2</sub> environment by an optical microscope, a FTIR, and MicrOmega, a near-infrared (0.99-3.65  $\mu\text{m}$ ) hyperspectral microscope. MicrOmega acquires images of 256x250 pixels with a spatial resolution of 22.5  $\mu\text{m}$ . The total field of view covers ~5.7x5.7mm<sup>2</sup> [3]. The first spectral characterization of the bulk samples within the Curation Facility [4,5] showed that the grains are extremely dark and exhibit absorption features at 2.72  $\mu\text{m}$ , 3.1  $\mu\text{m}$  and 3.4  $\mu\text{m}$  due to phyllosilicates, NH-rich compounds, and organics and/or carbonates respectively. The ~2.7  $\mu\text{m}$  feature was also observed on the asteroid's surface by the NIRS3 spectrometer [6]. In addition to the bulk samples, observations of individual grains, extracted from the bulks, were performed with MicrOmega. We investigate here the variations of the ~2.7  $\mu\text{m}$  feature at different scales, from the millimeter scale to the hundred microns scale, on 177 grains (typical size 1-7 mm) from chambers A and C.

In order to extract an average spectrum of each grain but also to delimit the region of interest to study the spectral heterogeneities inside the grains, we developed a procedure using thermal emission maps measured by MicrOmega. First, each grain was isolated from the rest of the field of view (the sample holder) thanks to their difference in terms of thermal emission. Then, we performed a study of the ~2.7 $\mu\text{m}$  band at two different scales. On one hand, all pixels within the mask were averaged to obtain the millimeter scale spectrum of each grain. On the other hand, to better understand the variations at millimeter scale, we looked at smaller scales (<200  $\mu\text{m}$ ) to highlight possible heterogeneities within the grains. Two spectral parameters were calculated to characterize the ~2.7  $\mu\text{m}$  OH feature: the peak position was estimated using a gaussian fit, and the band depth was calculated between the minimum of reflectance and a linear continuum.

At millimeter scale, the position of the ~2.7  $\mu\text{m}$  OH feature is consistent with the position found in highly aqueously altered carbonaceous chondrites [7]. Contrary to the bulk spectra where the ~2.7  $\mu\text{m}$  OH feature was very similar between the two chambers [5], the position of the band varies within an interval of 10 nm at individual grain scale and the peak position distribution varies between the two chambers: there is an excess of grains from chamber A with a position at longer wavelength. Another difference is that the band depth of the grains varies within a larger range in chamber A than in chamber C. The analysis at smaller scales (<200  $\mu\text{m}$ ) is still ongoing and will be presented at the time of the conference.

We will discuss the spectral differences between the collected grains, in particular between chambers A and C, and what information they carry about the composition of phyllosilicates and the space weathering processes affecting Ryugu's surface materials. Indeed, the OH feature position can change with the Mg/Fe ratio in phyllosilicates [8]. Moreover, space weathering experiments on carbonaceous chondrites [9] have shown that the band position was shifted towards longer wavelength after irradiation. The slight variation of band position we observe at the grain scale is consistent with the shift observed on Ryugu's surface spectra, between the artificial crater and the surrounding surface [10]. We expect that the smaller scale analysis will give hints on the involved processes.

### References

[1] Tachibana et al. (2020) LPS XXXXXI Abstract #2027. [2] Arakawa et al. (2017) Space Sci. Rev. 208, 187-212. [3] Bibring et al. (2017) Space Sci. Rev. 208, 401-412. [4] Yada et al. (2022) Nat Astron, 6, 214-220. [5] Pilorget et al. (2022) Nat Astron,

6, 221-225. [6] Kitazato et al. (2019) *Science*, 364, 272-275. [7] Takir et al. (2013) *M & PS* 48, 1618-1637. [8] Besson and Drits (1997), *CCM*, 45, 158. [9] Lantz et al. (2017) *Icarus* 285, 43-57. [10] Kitazato et al. (2021) *Nat Astron*, 5, 246-250.

## Organics in Ryugu samples, from MicrOmega and FTIR analyses within the ISAS curation facility

<sup>1</sup>Bibring, J.-P.; <sup>2,3</sup>Hatakeda, K.; <sup>1</sup>Brunetto, R.; <sup>1</sup>Baklouti, D.; <sup>1</sup>Carter, J.; <sup>1,4</sup>Pilorget, C.; <sup>1</sup>Loizeau, D.; <sup>2</sup>Yogata, K.; <sup>2,5</sup>Okada, T.; <sup>2</sup>Yada, T.; <sup>2,5</sup>Usui, T. and the IAS and ISAS MicrOmega Curation Team.

<sup>1</sup>IAS, Université Paris-Saclay, CNRS, France; <sup>2</sup>Institute of Space and Astronautical Science, Japan Aerospace Exploration Agency; <sup>3</sup>Marine Works Japan, Ltd; <sup>4</sup>Institut Universitaire de France; <sup>5</sup>University of Tokyo, Bunkyo, Tokyo 113-0033, Japan

Within the ISAS/JAXA facility, in which all samples collected by the Hayabusa 2 JAXA are maintained preserved from any terrestrial contamination [1], the MicrOmega instrument [2] has analyzed bulk samples from both collection sites, spread onto 6 main dishes, as well as hundreds of grains extracted from them. Two features show up in the NIR (0.99  $\mu\text{m}$  to 3.6  $\mu\text{m}$ ) spectra of essentially all grains, as acquired by MicrOmega: one, peaked around the 2.7  $\mu\text{m}$ , is diagnostic of OH stretch, primarily within the matrix material [3] while a second one, at  $\sim$ 3.4  $\mu\text{m}$ , is due to either or both carbonates [4] and organics [5]. This paper focusses on the later one, with updated results and interpretation.

Most of the  $\sim$ 3.4 organics-related features within MicrOmega spectra are peaked at 3.42  $\mu\text{m}$ , diagnostic of  $\text{CH}_2$  asymmetric stretch, with less significant  $\text{CH}_3$  absorption, around 3.38  $\mu\text{m}$  (asymmetric) nor 3.45 (symmetric), pointing at aliphatic methylenic moieties, with high  $\text{CH}_2/\text{CH}_3$ . MicrOmega spectra of a number of grains exhibit several other features, in a variety of intensities, often coupled with the 3.42  $\mu\text{m}$  and/or among themselves, primarily peaked around 2.9  $\mu\text{m}$ , 3.05  $\mu\text{m}$ , 3.25  $\mu\text{m}$ , 3.55  $\mu\text{m}$ . The candidate functional groups they are diagnostic of, are: aldehyde, alcohol, organic acid, amine and amide, and aromatics. The recent spectral upgrade of the FTIR within the curation facility, ranging up to 8.5  $\mu\text{m}$ , has demonstrated, through preliminary analyses of the larger grain of the collection (C9000,  $> 1$  cm wide), the potential of joined MicrOmega/FTIR measurements on the same grain.

Specifically, the FTIR provides means to discriminate between distinct potential compounds in two spectral domains: 5.2-6.2  $\mu\text{m}$ , and 6.8-7.8  $\mu\text{m}$ . Noticeably, C=O bonds (absorptions peaked at  $\sim$ 5.8  $\mu\text{m}$ ) can be distinguished from C=C bonds (absorptions peaked at  $\sim$ 6.2  $\mu\text{m}$ ). In addition, in a few spots, a critical feature shows up around 4.7  $\mu\text{m}$ , potentially tracing nitrile ( $-\text{C}\equiv\text{C}-$ ) or cyanate ( $\text{O}=\text{C}=\text{N}^+$ ). In addition to N-rich compounds, P-rich bonds [6] could be confirmed and characterized by FTIR.

We shall review all measurements performed up to now, by both MicrOmega and the upgraded FTIT within the curation facility, and discuss them in the frame of the evolution of the pristine organic constituents within Ryugu.

### References

- [1] Yada et al. (2022) Nat Astron, 6, 214-220
- [2] Pilorget et al. (2022) Nat Astron, 6, 221-225
- [3] LePivert et al. 2022, this symposium
- [4] Loizeau et al. 2022, this symposium
- [5] Carter et al. (2022) 53rd LPSC contrib. N°1495
- [6] Pilorget et al. 2022, this symposium

## MicrOmega detections of carbonates in Ryugu returned samples within the Hayabusa2 JAXA Extraterrestrial Curation Center

Loizeau, D.<sup>1</sup>; Pilorget, C.<sup>1</sup>; Riu, L.<sup>2</sup>; Brunetto, R.<sup>1</sup>; Bibring, J.-P.<sup>1</sup>; Nakato, A.<sup>3</sup>; Aléon-Toppani, A.<sup>1</sup>; Hatakeda, K.<sup>3</sup>; Yogata, K.<sup>3</sup>; Carter, J.<sup>1</sup>; Le Pivert-Jolivet, T.<sup>1</sup>; Yada, T.<sup>3</sup>; Okada, T.<sup>3</sup>; Usui, T.<sup>3</sup>; Langevin, Y.<sup>1</sup>; Lantz, C.<sup>1</sup>; Baklouti, D.<sup>1</sup>; Miyazaki, A.<sup>3</sup>; Nishimura, M.<sup>3</sup>; Nagashima, K.<sup>3</sup>; Kumagai, K.<sup>3</sup>; Hitomi, Y.<sup>3</sup>; Sugiyama, Y.<sup>3</sup>; Abe, M.<sup>3</sup>; Saiki, T.<sup>3</sup>; Tanaka, S.<sup>3</sup>; Nakazawa, S.<sup>3</sup>; Tsuda, Y.<sup>3</sup>; Watanabe, S.<sup>4</sup>;

<sup>1</sup>*Institut d'Astrophysique Spatiale, Université Paris-Saclay, CNRS, France*, <sup>2</sup>*ESAC, ESA, Madrid, Spain*,

<sup>3</sup>*Institute of Space and Astronautical Science, Japan Aerospace Exploration Agency, Japan*,

<sup>4</sup>*Nagoya University, Nagoya 464-8601, Japan*

The Ryugu samples brought back by the Hayabusa2 spacecraft in December 2020 have been delivered to the JAXA Extraterrestrial Curation Center [1, 2]. Bulk samples and then sub-bulks and individual grains have been picked up and stored into sapphire dishes, weighted, and analyzed with an optical microscope, FTIR spectroscopy, and MicrOmega hyperspectral imaging [3] for initial description within the curation facility [2]. The MicrOmega instrument used in the JAXA Extraterrestrial Curation Center is a NIR hyperspectral microscope. This configuration allows a mineralogical characterization of pristine Ryugu samples, as they have never been exposed to terrestrial environment.

MicrOmega has a total field of view of 5 mm x 5 mm, with resolution of ~22.5  $\mu\text{m}/\text{pixel}$  in the focal plane. It covers the spectral domain from 0.99  $\mu\text{m}$  to ~3.6  $\mu\text{m}$ . Its capabilities enable the identification of organic matter and of different minerals in the returned samples [4]. Initial analyses with MicrOmega were first made on the bulk samples from chambers A and C of the Hayabusa2 returned capsule, and then on extracted individual grains and sub-bulks, each stored in their sapphire dishes. For this study, we analyzed MicrOmega data of ~180 extracted individual grains (a few mm in size) and 14 sub-bulks (all observed with MicrOmega within the Curation Center in 2021). This is a unique opportunity for mapping mineral and organic species over a very large set of samples from Ryugu.

In the spectral domain of MicrOmega, carbonates have a strong characteristic double absorption band in the 3.3-3.5  $\mu\text{m}$  area, accompanied by two other weaker bands around 2.5 and 2.3  $\mu\text{m}$ . The exact spectral position of these bands varies with the cation content of the carbonate. Iron-bearing carbonates also show a strong absorption below 1.5  $\mu\text{m}$ .

Detections of carbonates were made in grains included in the bulk samples from both chambers A and C. In the bulks, some small detached grains seem to be entirely carbonate-rich and are up to ~450  $\mu\text{m}$ , down to <50  $\mu\text{m}$  in size. In larger, extracted grains, carbonate inclusions are also detected, with sizes up to >500  $\mu\text{m}$  in a 3mm-sized grain, and down to <50  $\mu\text{m}$ .

Spectrally, two carbonate populations are detected: many detections, mostly <100  $\mu\text{m}$  in size, have spectral bands centered at 2.30, 2.50, and 3.30-3.43  $\mu\text{m}$ , similar to  $\text{CaMg}(\text{CO}_3)_2$  dolomite; and few detections, mostly >100  $\mu\text{m}$ , have bands at 2.32, 2.51, 3.31-3.45  $\mu\text{m}$  together with a strong absorption <1.5  $\mu\text{m}$ , similar to  $(\text{Mg,Fe})\text{CO}_3$  breunnerite. We also report 3 small detections (<50  $\mu\text{m}$  in size) with spectra with bands at 3.35-3.48  $\mu\text{m}$ , similar to  $\text{CaCO}_3$  calcite. Both dolomite and breunnerite-like areas are detected in samples from both chambers, but we record more detections from chamber C than from chamber A.

The largest detection was made on grain C0041, covering ~0.25  $\text{mm}^2$ , or ~10% of the visible surface of the grain. This grain is one of the grains with “White regions” as described in [5]. The carbonate inclusion shows a complex morphology with three branches, 100s  $\mu\text{m}$  long, around a main area. Spectra of this detection are breunnerite-like.

Another large and complex carbonate inclusion was detected in grain C0181. In this example, bright carbonate detections surround a darker, 300  $\mu\text{m}$  long carbonate inclusion that seem to correspond to a single crystal where both bright and dark carbonates correspond to breunnerite-like spectra.

Carbonates detected by MicrOmega are distributed in two main populations both different in composition and size/morphology, questioning the formation process or processes that led to this two populations. We did not detect any spatial transition from dolomite to breunnerite, that would have indicated a possible gradient during a single formation event. We propose two distinct formation processes: dolomites may have formed within small pores in the precursor material, limiting their size, very early in the solar system [6], while breunnerite may have formed in fractures between grains, possibly after an impact on Ryugu's parent body, or even triggered by the impact. At what scale these processes were distinct in time is still questionable.

### References

[1] Tachibana S. et al. (2021) LPS, XXXXXII, Abstract #1289. [2] Yada T. et al. (2021) *Nature Astronomy* 6, p.214-220. [3] Pilorget et al. (2021) *Nature Astronomy* 6, p.221-225. [4] Pilorget C. and Bibring J.-P. (2014) *PSS* 99, 7-18. [5] Nakato A. et al. (2021) *8th Hayabusa Symposium*. [6] McCain K. A. et al. (2022) *85th METSOC annual meeting*.

# Oxygen and carbon isotope compositions of Ryugu's carbonates: Constraints on the conditions of aqueous alteration

Wataru Fujiya<sup>1</sup>, Noriyuki Kawasaki<sup>2</sup>, Kazuhide Nagashima<sup>3</sup>, Conel M. O'D. Alexander<sup>4</sup>, Hisayoshi Yurimoto<sup>2</sup>, The Hayabusa2-initial-analysis chemistry team, and The Hayabusa2-initial-analysis core.

<sup>1</sup>Ibaraki University, <sup>2</sup>Hokkaido University, <sup>3</sup>University of Hawai'i at Mānoa, <sup>4</sup>Carnegie Institution for Science

The Hayabusa2 spacecraft collected CI-chondrite-like materials from the near-Earth asteroid 162173 Ryugu [1]. Ryugu materials are mainly composed of secondary minerals that formed by aqueous alteration, e.g., phyllosilicates, carbonates, sulfides, and oxides. In this study, we performed *in-situ* O and C isotope measurements of calcite (CaCO<sub>3</sub>) and dolomite (CaMg(CO<sub>3</sub>)<sub>2</sub>) in Ryugu samples A0058 and C0002 as well as the Ivuna meteorite to investigate the conditions of the aqueous alteration. We used secondary ion mass spectrometry (SIMS; CAMECA ims-1280HR) at Hokkaido University with a suite of dolomite-ankerite standards [2] and a calcite standard "UWC3" [3].

The  $\delta^{18}\text{O}$  values of the calcites (24‰ to 46‰) in C0002 and Ivuna show a larger variation than those of the dolomites in C0002, A0058, and Ivuna (26‰ to 31‰) (Fig. 1). The average  $\Delta^{17}\text{O}$  value of the C0002 and Ivuna calcites is  $1.37 \pm 0.40\text{‰}$  (2SE). The  $\Delta^{17}\text{O}$  values of the C0002, A0058, and Ivuna dolomites are systematically lower than those of the calcites, and the average  $\Delta^{17}\text{O}$  value of the dolomites ( $0.26 \pm 0.23\text{‰}$ , 2SE) is closer to the whole-rock values of two Ryugu samples [4] (0.30‰ and 0.58‰). Like the  $\delta^{18}\text{O}$  values, the dolomites in A0058, C0002, and Ivuna have a relatively narrow range of  $\delta^{13}\text{C}$  values from 67‰ to 75‰ (Fig. 2). On the other hand, the  $\delta^{13}\text{C}$  values of the calcites in C0002 and Ivuna are highly heterogeneous, ranging from 65‰ to 108‰, and they are commonly higher than those of the Ryugu and Ivuna dolomites.

If, when the carbonates precipitated they were in O and C isotope equilibrium with the aqueous fluid, their O and C isotope compositions would have been determined by the mass dependent equilibrium isotopic fractionation, which depends on temperature, between carbonates and water for O, and that between carbonates and dissolved CO<sub>3</sub><sup>2-</sup> (and other dissolved C-bearing chemical species) for C [5]. Thus, the O and C isotope compositions of carbonates would reflect those of water and CO<sub>3</sub><sup>2-</sup> as well as their formation temperatures. The  $\delta^{18}\text{O}$  variation of ~22‰ observed in the Ryugu calcites (Fig. 1) corresponds to formation temperatures that varied from 0 °C to 150 °C. However, the lack of a correlation between  $\delta^{18}\text{O}$  and  $\delta^{13}\text{C}$  values implies that variable formation temperatures alone cannot explain the observed  $\delta^{18}\text{O}$  and  $\delta^{13}\text{C}$  variations (Fig. 2). Rather it seems likely that both the  $\delta^{18}\text{O}$  value of water and the  $\delta^{13}\text{C}$  value of CO<sub>3</sub><sup>2-</sup> varied temporally. Because the  $\Delta^{17}\text{O}$  values of the fluids likely decreased as water-rock interaction progressed [6], the calcites with systematically higher  $\Delta^{17}\text{O}$  values should have formed from less "evolved" fluids and likely crystallized earlier than the dolomites (Fig. 1).

It seems likely that the temporal variation in the  $\delta^{13}\text{C}$  values of the C reservoirs and in their chemical speciation occurred due to a change of O fugacity ( $f\text{O}_2$ ). Oxygen fugacity varied along with the production of H<sub>2</sub> via the oxidation of Fe in metal and silicates by H<sub>2</sub>O and the subsequent escape of H<sub>2</sub> from the system. To see how the  $\delta^{13}\text{C}$  values of carbonates will change with varying  $f\text{O}_2$ , we consider a rather simple model, where gaseous CO<sub>2</sub> and CO and carbonates (and dissolved CO<sub>2</sub>, HCO<sub>3</sub><sup>-</sup>, and CO<sub>3</sub><sup>2-</sup>) are in C isotopic equilibrium and the CO<sub>2</sub>/CO ratio increases with increasing  $f\text{O}_2$ . At first, the CO<sub>2</sub>/CO ratio may have been characterized by that of the accreted ices, which may be around unity or higher as observed in cometary ices [7]. We assume that the  $\delta^{13}\text{C}$  value of the bulk gas (CO<sub>2</sub>+CO),  $\delta^{13}\text{C}_{\text{bulk}}$ , is constant regardless of the CO<sub>2</sub>/CO ratio. Because the C isotopic fractionation factor between CO<sub>2</sub> and CO is positive at any temperature, e.g., 93‰ at 0 °C [8], both the  $\delta^{13}\text{C}$  values of CO<sub>2</sub> and CO will decrease monotonically with increasing  $f\text{O}_2$  to keep  $\delta^{13}\text{C}_{\text{bulk}}$  constant, and the  $\delta^{13}\text{C}$  values of carbonates will also decrease (Fig. 2). In this context, the dolomites with lower  $\delta^{13}\text{C}$  values likely formed at higher  $f\text{O}_2$  and/or temperature than the calcites. This, combined with the O isotope signatures of the carbonates, implies that the calcites formed during prograde alteration over wide ranges of  $f\text{O}_2$  and temperature, whereas the dolomites formed later from peak temperature to retrograde cooling when the aqueous fluids and silicates approached O isotope equilibrium [9].

## References:

- [1] Yokoyama T. et al. *Science*, 10.1126/science.abn7850 (2022) [2] Śliwiński M. G. et al. *Geostand. Geoanal. Res.* 40, 173-184 (2016). [3] Kozdon R. et al. *Chem. Geol.* 258, 327-337 (2009). [4] Tang H. et al. *Sci. Adv.*, submitted. [5] Alexander, C. M. O'D. et al. *Meteorit. Planet. Sci.* 50, 810-833 (2015). [6] Clayton R. N. & Mayeda T. K. *Earth Planet. Sci. Lett.* 67, 151-161 (1984). [7] Ootsubo T. et al. *Astrophys. J.* 752, 15 (2012). [8] Richet P. et al. *Ann. Rev. Earth Planet. Sci.* 5, 65-110 (1977). [9] Nagashima et al. this meeting.

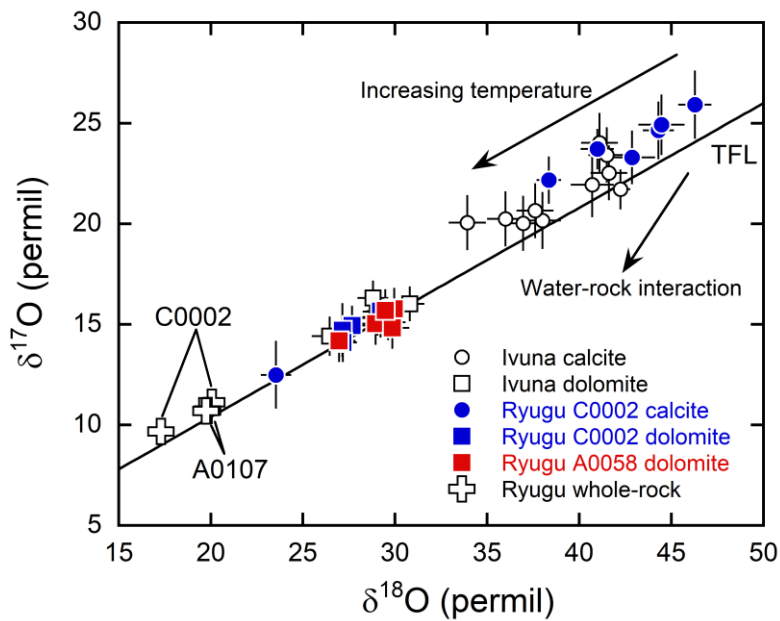


Figure 1. Oxygen isotope compositions of the calcite and dolomite grains in Ryugu and Ivuna samples.

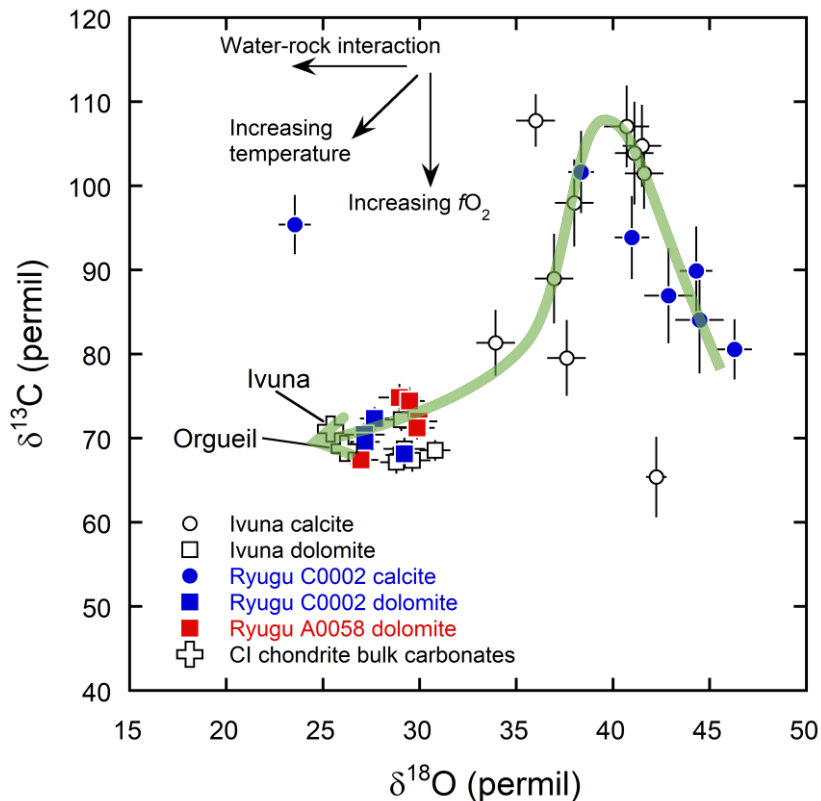


Figure 2. Comparison between C and O isotope compositions of the calcite and dolomite grains in Ryugu and Ivuna samples. A putative evolutionary trend of  $\delta^{18}\text{O}$  and  $\delta^{13}\text{C}$  values is shown by the green arrow.

**The Hayabusa2-initial-analysis chemistry team:** T. Yokoyama, K. Nagashima, Y. Abe, J. Aléon, C.M.O'D. Alexander, S. Amari, Y. Amelin, K. Bajo, M. Bizzarro, A. Bouvier, R. W. Carlson, M. Chaussidon, B.-G. Choi, N. Dauphas, A.M. Davis, T. Di Rocco, W. Fujiya, R. Fukai, I. Gautam, M.K. Haba, Y. Hibiya, H. Hidaka, H. Homma, P. Hoppe, G.R. Huss, K. Ichida, T. Iizuka, T.R. Ireland, A. Ishikawa, M. Ito, S. Itoh, N. Kawasaki, N.T. Kita, K. Kitajima, T. Kleine, S. Komatani, A.N. Krot, M.-C. Liu, Yuki Masuda, K.D. McKeegan, M. Morita, K. Motomura, F. Moynier, I. Nakai, A. Nguyen, L. Nittler, M. Onose, A. Pack, C. Park, L. Piani, L. Qin, S.S. Russell, N. Sakamoto, M. Schönbachler, L. Tafla, H. Tang, K. Terada, Y. Terada, T. Usui, S. Wada, M. Wadhwa, R.J. Walker, K. Yamashita, Q.-Z. Yin, S. Yoneda, E.D. Young, H. Yui, A.-C. Zhang, H. Yurimoto.

**The Hayabusa2-initial-analysis core:** S. Tachibana, T. Nakamura, H. Naraoka, T. Noguchi, R. Okazaki, K. Sakamoto, H. Yabuta, H. Yurimoto, Y. Tsuda, S. Watanabe.

# Extraterrestrial Amino Acids and Amines Identified in Asteroid Ryugu Samples Returned by the Hayabusa2 Mission

Eric T. Parker<sup>1</sup>, Hannah L. McLain<sup>1,2,3</sup>, Daniel P. Glavin<sup>1</sup>, Jason P. Dworkin<sup>1</sup>, Jamie E. Elsila<sup>1</sup>, José C. Aponte<sup>1,2,3</sup>, Hiroshi Naraoka<sup>4</sup>, Yoshinori Takano<sup>5</sup>, Shogo Tachibana<sup>6</sup>,

The Hayabusa2-initial-analysis SOM team, The Hayabusa2- initial-analysis core

<sup>1</sup>*Astrobiology Analytical Laboratory, Solar System Exploration Division, NASA Goddard Space Flight Center, Greenbelt, MD 20771, U.S.A.*

<sup>2</sup>*Center for Research and Exploration in Space Science and Technology (CRESST), NASA Goddard Space Flight Center, Greenbelt, MD 20771, U.S.A.;* <sup>3</sup>*Department of Physics, The Catholic University of America, Washington, D.C. 20064, U.S.A.;*

<sup>4</sup>*Department of Earth and Planetary Science, Kyushu University, Nishi-ku, Fukuoka, 819-0395, Japan;* <sup>5</sup>*Biogeochemistry Research Center (BGC), Japan Agency for Marine-Earth Science and Technology (JAMSTEC), Yokosuka, Kanagawa, 237-0061, Japan;* <sup>6</sup>*UTokyo Organization for Planetary and Space Science (UTOPS), The University of Tokyo, 7-3-1 Hongo, Tokyo 113-0033, Japan*

Analyses of amino acids and aliphatic amines were performed on the hot water extracts of two asteroid Ryugu samples returned by the JAXA Hayabusa2 mission. The two samples were A0106, which was comprised of surface material, and C0107, which was comprised of both surface and possible subsurface material. Prior to amino acid analysis, portions of each sample extract underwent acid vapor hydrolysis, while other portions remained unhydrolyzed to allow for a respective comparison between bound and free amino acids. Subsequently, these extracts were derivatized with *o*-phthalaldehyde/*N*-acetyl-L-cysteine, a chiral, fluorescent tag that enhances analytical specificity and sensitivity for primary amines, and then analyzed using ultrahigh performance liquid chromatography with fluorescence detection and high-resolution mass spectrometry. Prior to the analysis of aliphatic amines, separate portions of each sample extract were derivatized with AccQ•Tag, a fluorescent tag that is insensitive to salts and targets primary amines and select secondary amines, and then analyzed by ultraperformance liquid chromatography with fluorescence detection and time-of-flight mass spectrometry. The analyses performed here focused on the abundances and relative distributions of amino acids and aliphatic amines, as well as determining the enantiomeric compositions of detected chiral amino acids. For contamination control and background subtraction purposes, procedural and analytical blanks were processed and analyzed in parallel with the Ryugu samples.

In total, 13 amino acids were detected and quantitated here. Five additional amino acids were tentatively identified, but not quantitated. Abundances of individual amino acids of the C<sub>2</sub> – C<sub>6</sub> variety were measured to vary between 0.02 and 15.8 nmol g<sup>-1</sup>. Among those amino acids identified, several were non-protein amino acids that are uncommon in biology. These included β-aminoisobutyric acid (β-AIB) and β-amino-*n*-butyric acid (β-ABA), which were measured to be racemic or very nearly racemic, suggesting that these species were likely to be indigenous to the sample and extraterrestrial in nature. While trace quantities of select protein amino acids were found to be enriched in the L-enantiomer, elevated abundances of racemic, free alanine were observed, indicating that the Ryugu sample studied here were exposed to minimal terrestrial contamination.

The analyses of aliphatic amines revealed four species of the C<sub>1</sub> – C<sub>3</sub> variety, which were identified and measured above background levels. These aliphatic amines were methylamine, ethylamine, isopropylamine, and propylamine, in order of descending abundances. These aliphatic amine species were individually measured at abundances ranging from 0.05 – 34.14 nmol g<sup>-1</sup> in the unhydrolyzed hot water extracts of Ryugu samples A0106 and C0107.

It has been reported that Ryugu samples are chemically similar to CI-type chondrites [1,2]. However, the abundances and relative distributions of amino acids and aliphatic amines in Ryugu are strikingly different from those of CI1.1/2.0 Orgueil. More specifically, CI1.1/2.0 Orgueil contains upwards of 5.6x the total abundance of amino acids as Ryugu, and more than 5x the total abundance of aliphatic amines as Ryugu. These observed abundance differences could be caused by discrepancies in alteration conditions experienced by the parent bodies of Orgueil and Ryugu, or variabilities in original parent body chemical conditions. Additionally, it is plausible the lower overall abundances of amino acids and amines in the near-surface samples collected by Ryugu may be due to the loss of these compounds, or their volatile precursors, via such factors as space weathering and solar heating in a hard vacuum environment. These possible loss mechanisms are worthy of further exploration. Regarding amino acid distributions observed in Ryugu, α-amino acids, which could have been generated by the Strecker cyanohydrin synthesis, were identified, along with β-, γ-, and δ-amino acids. Examples of the latter included C<sub>3</sub> – C<sub>5</sub> straight-chain *n*-ω-amino acids. The observed amino acid distribution indicates that more than one formation mechanism occurred on the Ryugu parent body and was responsible for the amino acids reported here. Lastly, the analytical techniques used here were sufficiently sensitive to detect and quantify the target analytes under the limited sample mass conditions of the current work, which offers strong evidence that these methods will likely perform similarly well when applied to the analyses of amino acids and aliphatic amines in asteroid Bennu samples returned by the NASA OSIRIS-REx mission in September 2023.

## References

[1] Yada, T. et al. (2022) *Nature Astronomy*, 6, 214-220. [2] Yokoyama, T. et al. (2022) *Science*, eabn7850.

**The Hayabusa2-initial-analysis SOM team:** Hiroshi Naraoka, Yoshinori Takano, Jason P. Dworkin, Kenji Hamase, Aogu Furusho, Minako Hashiguchi, Kazuhiko Fukushima, Dan Aoki, José C. Aponte, Eric T. Parker, Daniel P. Glavin, Hannah L. McLain, Jamie E. Elsila, Heather V. Graham, John M. Eiler, Philippe Schmitt-Kopplin, Norbert Hertkorn, Alexander Ruf, Francois-Regis Orthous-Daunay, Cédric Wolters, Junko Isa, Véronique Vuitton, Roland Thissen, Nanako O. Ogawa, Saburo Sakai, Toshihiro Yoshimura, Toshiki Koga, Haruna Sugahara, Naohiko Ohkouchi, Hajime Mita, Yoshihiro Furukawa, Yasuhiro Oba, Yoshito Chikaraishi.

**The Hayabusa2-initial-analysis core:** Shogo Tachibana, Tomoki Nakamura, Hiroshi Naraoka, Takaaki Noguchi, Ryuji Okazaki, Kanako Sakamoto, Hikaru Yabuta, Hisayoshi Yurimoto, Yuichi Tsuda, Sei-ichiro Watanabe.

# Carbon dust, from the ISM to the Solar System

E. Dartois<sup>1</sup>

<sup>1</sup>*Institut des Sciences Moléculaires d'Orsay (ISMO), UMR8214, CNRS, Université Paris-Saclay 91405 Orsay Cedex, France*

The spectral signatures of interstellar medium dust grains reveal a great diversity of allotropes. Astronomical observations give access to the molecular functionalities of these solids, setting constraints on the composition of organic solids and molecules in the cycling of matter in the Galaxy. Some of these grains and molecules can be reproduced in the laboratory. Other signatures still await for more precise identification of their carriers phases. Laboratory analogues help in constraining their physico-chemical composition and evolution under the harsh galactical radiation environments. This talk will particularly focus on dust materials from the far space environments, from diffuse ISM to protoplanetary disks. We'll present some commonalities and differences between materials found in the Solar System, protoplanetary disks and Interstellar dust.

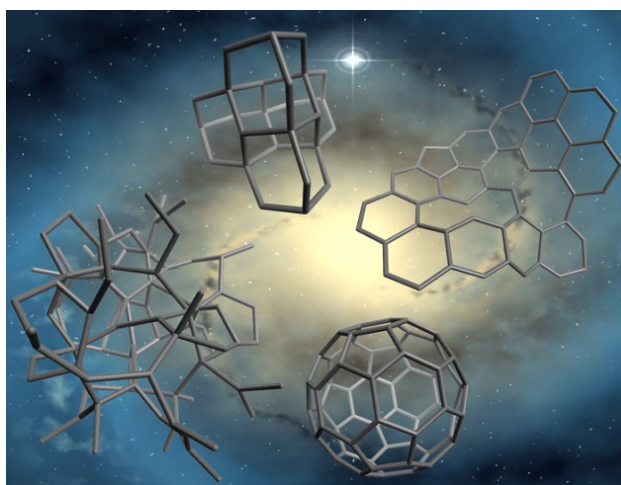


Figure 1. Interstellar carbon allotropes (from Dartois et al. 2019).

## References

- [1] Dartois, E., Charon, E., Engrand, C., Pino, T., Sandt, C. 2020. *Mechanochemical synthesis of aromatic infrared band carriers. The top-down chemistry of interstellar carbonaceous dust grain analogues.* *Astronomy and Astrophysics* 637. doi:10.1051/0004-6361/202037725
- [2] Dartois, E. 2019. *Interstellar carbon dust.* *C*, 5(4), 80.
- [3] Dartois, E. and 17 colleagues 2015. *Interstellar and interplanetary solids in the laboratory.* *Bulletin de la Societe Royale des Sciences de Liege* 84, 7–14.